DTIC FILE COPY

FINAL REPORT ON
AFOSR CONTRACT F49620-83-C-0064

Steven A. Orszag, Principal Investigator
Department of Mathematics
MIT
Cambridge, MA 02139

Volume 1

DTIC
ELECTE
MAR 0 1 1988
S   D
    H

88   3   1   2 0 0

SECURITY CLASSIFICATION OF THIS PAGE

ADA191253

REPORT DOCUMENTATION PAGE

1a. REPORT SECURITY CLASSIFICATION Unclassified	1b. RESTRICTIVE MARKINGS
2a. SECURITY CLASSIFICATION AUTHORITY	3. DISTRIBUTION/AVAILABILITY OF REPORT Approved for public release; distribution is unlimited
2b. DECLASSIFICATION/DOWNGRADING SCHEDULE	

4. PERFORMING ORGANIZATION REPORT NUMBER(S)	5. MONITORING ORGANIZATION REPORT NUMBER(S) AFOSR·TR· 87-1390

6a. NAME OF PERFORMING ORGANIZATION MIT	6b. OFFICE SYMBOL (If applicable)	7a. NAME OF MONITORING ORGANIZATION AFOSR/NA

6c. ADDRESS (City, State and ZIP Code) Department of Mathematics MIT Cambridge, MA 02139	7b. ADDRESS (City, State and ZIP Code) Building 410, Bolling AFB DC 20332-6448.

8a. NAME OF FUNDING/SPONSORING ORGANIZATION AFOSR/NA	8b. OFFICE SYMBOL (If applicable) NA	9. PROCUREMENT INSTRUMENT IDENTIFICATION NUMBER F49620-83-C-0064

8c. ADDRESS (City, State and ZIP Code) Bld 410	10. SOURCE OF FUNDING NOS.			
Bolling Air Force Base Washington, DC 20332-6448 .	PROGRAM ELEMENT NO. 61102F	PROJECT NO. 2307	TASK NO. A2	WORK UNIT NO.

11. TITLE (Include Security Classification) Final Report on AFOSR Contract F49620-83-C-0064

12. PERSONAL AUTHOR(S)
- Steven A. Orszag

13a. TYPE OF REPORT Final Report	13b. TIME COVERED FROM 2/1/83 TO 11/30/84	14. DATE OF REPORT (Yr., Mo., Day) May, 1987	15. PAGE COUNT 130

16. SUPPLEMENTARY NOTATION

17.	COSATI CODES		18. SUBJECT TERMS (Continue on reverse if necessary and identify by block number)
FIELD	GROUP	SUB. GR.	Turbulence, Numerical Simulation

19. ABSTRACT (Continue on reverse if necessary and identify by block number)

We summarize work done under AFOSR Contract F49620-83-C-0064. The major results include: development of renormalization group techniques for large-eddy simulations of turbulent flows, the first direct numerical simulation of turbulent spots in channel and boundary-layer flows, the further development of spectral methods for turbulence simulations, the identification of secondary instability modes in free shear layers, the development of an efficient multi-grid marching method for solution of the parabolized Navier-Stokes equations, a mathematical analysis of boundary conditions for the parabolized compressible Navier-Stokes equations, the further development of a method to improve numerical solution of singular perturbation problems by use of asymptotic approximations.

20. DISTRIBUTION/AVAILABILITY OF ABSTRACT UNCLASSIFIED/UNLIMITED ☒ SAME AS RPT. ☒ DTIC USERS ☐	21. ABSTRACT SECURITY CLASSIFICATION Unclassified

22a. NAME OF RESPONSIBLE INDIVIDUAL Dr James M McMichael	22b. TELEPHONE NUMBER (Include Area Code) (202) 767-4936	22c. OFFICE SYMBOL AFOSR/NA

DD FORM 1473, 83 APR   EDITION OF 1 JAN 73 IS OBSOLETE.

SECURITY CLASSIFICATION OF THIS PAGE

FINAL REPORT ON AFOSR CONTRACT F49620-83-C-0064

Steven A. Orszag, Principal Investigator

Department of Mathematics

MIT

Cambridge, MA 02139

In the attached papers, we summarize work done on this research project. The major results include:

1.   Development of renormalization group techniques for large-eddy simulations of turbulent flows.

2.   The first direct numerical simulation of turbulent spots in channel and boundary layer flows.

3.   The further development of spectral methods for turbulence simulations.

4.   The identification of secondary instability modes in free shear layers.

5.   The development of an efficient multi-grid marching method for solution of the parabolized Navier-Stokes equations.

6.   A mathematical analysis of boundary conditions for the parabolized compressible Navier-Stokes equations.

7.   The further development of a method to improve numerical solution of singular perturbation problems by use of asymptotic approximations.

Further details are given in the attached papers.

List of Papers

M. Israeli and P. Bar-Yoseph, Numerical Solution of Multi-Dimensional Diffusion-Convection Problems by Asymptotic Corrections, in Proc. Fifth GAMM-Conference on Num. Meth. in Fl. Mech., Friedr. Vieweg & Sohn, 1984.

S.A. Orszag, Instabilities and Turbulence, in Turbulence and Chaotic Phenomena in Fluids, (ed. by T. Tatsumi), North-Holland (1984).

V. Yakhot and S.A. Orszag, Renormalization Group Formulation of Large Eddy Simulation, in Non-Linear Dynamics of Transcritical Flows, (ed. by H. L. Jordan), Springer (1985).

S.A. Orszag, Lectures on Spectral Methods for Turbulence Computations, in Proc. of International School of Physics 'Enrico Fermi', (ed. by M. Ghil), North-Holland (1985).

M. Israeli, Marching Iterative Methods for the Parabolized and Thin Layer Navier-Stokes Equations, NASA Contractor Report 178028/ICASE Report No. 85-60 (1985).

E.T. Bullister and S.A. Orszag, Numerical Simulation of Turbulent Spots in Channel and Boundary Layer Flows. J. Sci. Comp., in press.

M. Rosenfeld and M. Israeli, Numerical Solution of Incompressible Flows by a Marching Multigrid Nonlinear Method, AIAA Journal **25**, 5 (1987).

Maurizio Pandolfi/Renzo Piva (Eds.)

Proceedings of the Fifth GAMM-Conference on Numerical Methods in Fluid Mechanics

Rome, October 5 to 7, 1983

With 263 Figures

Reprint

V

Friedr. Vieweg & Sohn   Braunschweig/Wiesbaden

NUMERICAL SOLUTION OF MULTI-DIMENSIONAL DIFFUSION-CONVECTION PROBLEMS
BY ASYMPTOTIC CORRECTIONS

M. Israeli* and P. Bar-Yoseph**

Technion - Israel Institute of Technology
Haifa, Israel

SUMMARY

The Booster Method for improvement of the numerical solution of par-
tial differential equations by the addition of asymptotic corrections to
the right hand side is presented. It is applied here to the diffusion-
convection equation for the case of 'small' diffusion. The correction
terms were used in finite difference and finite element schemes. The
finite element results were used as reference for checking the performance
of the finite difference schemes. Excellent results were obtained without
the use of upstreaming or artificial diffusion. Theoretical expectations
were confirmed.

1. INTRODUCTION

Singularly perturbed initial and boundary value problems for partial
differential equations appear in various fields of application such as
fluid dynamics, heat transfer, transport of atmospheric pollution, etc. In
particular, such equations appear in diffusion-convection processes. Often
the (normalized) diffusion coefficient ε becomes small, and thin boundary
or interior layers appear within the region of interest. Consequently,
these problems become increasingly difficult to solve numerically by dis-
cretization methods.

We would like to avoid the use of a prohibitively large number of grid
points, as required for resolution by straightforward numerical methods
when ε decreases. To this end, several approaches are possible, such as
the use of nonuniform meshes, adaptive techniques, positive type schemes,
etc. The question of applicability of such schemes to multi-dimensional
problems is presently open.

A different approach is motivated by classical singular perturbation
methods where 'inner' and 'outer' solutions are combined to give approxi-
mate solutions. These solutions become more accurate as the equations
become stiffer, however, the error is fixed for a given ε and cannot be
improved or estimated reliably in most cases of interest.

The Booster Method attempts to combine the asymptotic approach, with
known discretization methods, in order to obtain a numerical method which
improves when ε becomes smaller. At the same time, it keeps the proper-
ty that the error can be made arbitrarily small for any fixed ε by refin-
ing the computational mesh (Israeli and Ungarish [1],[2]). For the one-
dimensional case, we were able to prove that an improvement by a factor of
ε^{n+1} can be obtained where ε is the 'small' parameter and n is the
order of the asymptotic approximation used (Israeli and Ungarish [2]). We
expect similar behaviour in the multidimensional case [1].

In the present paper, we investigate a multi-dimensional application
to diffusion-convection problems.

---

* Department of Computer Science, Technion.
** Department of Mechanical Engineering, Technion.

2. FORMULATION

We consider the transport of a quantity q in a rectangular region. The normalized partial differential equation is

$$L(q) \equiv -\epsilon\nabla^2 q + \vec{V} \cdot \nabla q = 0 \quad . \tag{1}$$

In the present application the velocity field $\vec{V}$ is assumed to be known and q is specified on the boundaries. This problem was often used as a test case for various finite difference and finite element methods of solution and it is well known that most methods fail as the cell Reynolds number $(|\vec{V}|h)/\epsilon$ becomes larger than $O(1)$ (here h is a representative mesh size). For example centered schemes develop unphysical oscillations in space, while uncentered schemes have unacceptable artificial diffusion and are of lower order over the same computational stencil.

The Booster Method uses an asymptotic approximation $\tilde{q}(x,y)$ to the solution $q(x,y)$ in order to reduce the truncation error in the numerical scheme.

The 'usual' numerical solution $Q(x,y)$ (defined only at grid points) is obtained from

$$L_N(Q) = f \quad , \tag{2}$$

where L_N is the discrete approximation to the differential operator L. The improved numerical solution $\bar{Q}$ is obtained from

$$L_N(\bar{Q}) = f + L_N(\tilde{q}) - L(\tilde{q}) \quad . \tag{3}$$

Here $L(\tilde{q})$ is the differential operator applied to the approximate solution. Thus the Booster Method applies an asymptotic correction to the right hand side of the equation and therefore requires a negligible amount of extra work. It can be used with any numerical scheme without modification in the method of solution.

The same basic approach of using asymptotic corrections to the right hand side can be used to improve the Standard Finite Element (SFE) method. The resulting Asymptotic Finite Element (AFE) method is described briefly in the following; for details see Bar-Yoseph and Israeli [4],[5].

Suppose that the unit square is divided into elements and that the variation of q within the given region is approximated by

$$Q(\vec{x}) \approx N_i(\vec{x})Q_i \quad , \tag{4}$$

where Q_i is the value of the approximate solution at the i-th nodal point and N_i is the corresponding global trial function (we use the summation convention, with summation over the nodes within the given region). The Bubnov-Galerkin finite element scheme of eq. (1) is given by

$$\epsilon(\nabla^T N_j, \nabla N_i Q_i)_h + (N_j, \vec{V} \cdot \nabla N_i Q_i)_h = (N_j, f)_h \quad , \quad j = 1,2,\ldots,m \quad , \tag{5}$$

where m is the number of inner nodal points and $(\cdot,\cdot)$ denotes the usual inner product in $L_2(\Omega)$. The subscript h in $(\cdot,\cdot)_h$ denotes an approximation to $(\cdot,\cdot)$ obtained by a quadrature rule.

Our corresponding asymptotic finite element (AFE) scheme for eq. (1) is the following

$$\epsilon(\nabla^T N_j, \nabla N_i \bar{Q}_i)_h + (N_j, \vec{V} \cdot \nabla N_i \bar{Q}_i)_h = (N_j, f)_h$$

$$+ \{\epsilon(\nabla^T N_j, \nabla N_i \tilde{q}_i)_h + (N_j, \vec{V} \cdot \nabla N_i \tilde{q}_i)_h - (N_j, L\tilde{q})\} \quad , \quad j = 1, 2, \ldots, m \quad , \quad (6)$$

where $\tilde{q}_i$ is the value of the asymptotic solution at the i-th nodal point. Here the terms included in the first line coincide with the SFE scheme, eq. (5), while the terms in the second line (in curled brackets) represent the correction term which is the essence of the present AFE scheme. This AFE scheme can also improve the pointwise error estimate of the SFE scheme by a factor of the $O(\epsilon^{n+1})$ [4].

Usually the finite element solution supplies values everywhere inside the elements via the interpolation (4). Applying the same interpolation using $\bar{Q}_i$ instead of Q_i will not give good results within the elements especially when there are no nodal points inside the boundary layers. One should use instead the interpolation

$$q(\vec{x}) \simeq \tilde{q}(\vec{x}) + N_i(\vec{x})(\bar{Q}_i - \tilde{q}_i)$$

which recovers the proper boundary layer behaviour.

3. ASYMPTOTIC SOLUTION

The approximation $q(x,y)$ can be obtained by the method of matched asymptotic expansions (Cole [3]). Such approximations usually satisfy the boundary conditions and become increasingly accurate as ϵ decreases. Often the error decreases like some power of ϵ depending on the number of terms used in the construction of the solution (see Table I).

We first construct the zeroth order asymptotic approximation from the outer solution q_o, where

$$\vec{V} \cdot \nabla q_o = 0 \quad , \quad (7)$$

and from the boundary layer q_b satisfying a one-dimensional boundary layer equation in the direction normal to the boundaries (where the flow exits the computational region). A complete zeroth order solution should also include corner regions, tangential regions, and boundary layers developing from discontinuities in boundary conditions. Restricting ourselves for now to continuous boundary conditions and constant velocity field not tangent to any boundary, we find that only the exit corner layer has to be included.

Equation (7) implies that the solution remains constant along streamlines, consequently it carries with it the q-values entering the computational region. The difference between these values and the values encountered at the exit forces the boundary layers.

We consider the flow in the unit square with vertices (0,0), (0,1), (1,0), (1,1). Let the components of $\vec{V}$ be u and v (both positive) and the differences of the exit boundary $x = 1$ and $y = 1$ be $f(y)$ and $g(x)$ respectively. Then the structure of the boundary layers will be

$$q_b = f(y)e^{u(x-1)/\epsilon} + g(x)e^{v(y-1)/\epsilon} - pe^{u(x-1)/\epsilon}e^{v(y-1)/\epsilon} \quad , \quad (8)$$

where $p = f(1) = g(1)$ and $f(0) = g(0) = 0$ by assumption.

The third term in (8) is the corner boundary layer and it satisfies the differential equation exactly (in this particular case). The approximation $\tilde{q}$ is obtained by adding q_o from (7) to q_b from (8). It is a

uniformly valid approximation in the square, and is easily adapted to particular cases. In our example $u = v = \sqrt{2}/2$ and the outer solution is

$$q_o = \sin\pi(x-y) \quad , \tag{9}$$

corresponding to the boundary conditions

$$q(x,0) = \sin\pi x; \quad q(0,y) = -\sin\pi y \quad . \tag{10}$$

On the other hand we take

$$q(x,1) = \sin\pi(x-1) + x, \quad q(1,y) = \sin\pi(1-y) + y \quad , \tag{11}$$

giving rise to $f(y) = y$ and $g(x) = x$, which satisfy the requirement of continuity on the boundary.

4. RESULTS

We solved the differential equation (1) in the unit square with the boundary conditions (10) and (11) on a net with 6, 12 and 24 equal intervals in the x and y directions. We used centered three-point differences for the first and second derivatives. As we do not have the exact solution for this problem, we used as reference a solution obtained with the AFE scheme employing a uniform mesh of 24×24 biquadratic Lagrangian elements (more details appear in [5]). The range of ϵ reproduced in the tables was $\epsilon = 0.01$, $\epsilon = 0.02$, $\epsilon = 0.05$.

As a seminorm we used a weighted average of the absolute value of the errors. A proper mix of interior and boundary layer points was obtained by taking only the 25 mesh points contained in a square near the corner $(1,1)$.

We observe that (Table I) the error in the asymptotic approximation $A(\epsilon,h)$ decreases roughly like ϵ. The error in the regular (Table III) numerical solution $N(\epsilon,h)$ decreases very slowly with h and increases as ϵ decreases.

We note first that the errors in Table II are in all cases smaller than the corresponding errors in Tables I and III. Moreover the analysis of [2] indicates that the error in the improved solution $B(\epsilon,h)$ should decrease with ϵ and h (Table II). In fact it should be proportional to the product of the previous errors. Table IV presents the ratio $K(\epsilon,h) = B(\epsilon,h)/((A(\epsilon,h)N(\epsilon,h)))$. We expect it to approach a constant, the fact that the values in Table IV are not far from unity makes the booster method quite attractive.

We note that the centered method is quite useless by itself. Our experience shows that the Booster Method works equally well with other schemes and other discretization methods.

ACKNOWLEDGEMENT

REFERENCES

[1] Israeli, M. and Ungarish, M.: Proceeding of the ICNMFD7, Stanford, 1980, Lecture Notes in Physics, 141, Springer-Verlag.

[2] Israeli, M. and Ungarish, M.: Numer. Math. 39, 309-324 (1982).

[3] Cole, J.D.: Perturbation Methods in Applied Mathematics, Waltham, Mass., Blaisdell Publ. Co., 1968.

[4] Bar-Yoseph, P. and Israeli, M.: An asymptotic finite element method for improvement of finite element solutions of boundary layer problems (to appear).

[5] Bar-Yoseph, P. and Israeli, M.: An asymptotic finite element method for 2-D convection-diffusion problems (in preparation).

INSTABILITIES AND TURBULENCE

Steven A. Orszag

Massachusetts Institute of Technology
Cambridge, Massachusetts 02139 USA

This paper gives an overview of recent nu-
merical studies of transition and turbulence in
incompressible shear flows. First, we summarize
features of a three-dimensional instability that
seems to be responsible for the early stages of
transition in planar shear flows. Then, we
describe some new results on the simulation of
turbulent spots in a channel flow and some new
ideas on the role of viscosity in producing
small-scale structures in turbulent flows. Fi-
nally, we discuss the problem of representing
the effects of sub-grid-scale motions in large-
eddy simulations of turbulence.

1. INTRODUCTION

Over the last few years, there has been progress in understand-
ing fundamental nonlinear processes in shear flows. In this paper,
I shall survey some results that have emerged from numerical studies
of transition and turbulence. I shall review for you three dif-
ferent aspects of these problems. First, I shall summarize results
on the basic instabilities that seem to be responsible for the onset
of chaos in these flows. These instabilities appear to be universal
in character and may explain many of the unifying features of tran-
sition. Second, I shall give some examples of progress in the nu-
merical simulation of high Reynolds number flows. Finally, I will
give a synopsis of new ideas for sub-grid-scale closures of huge
Reynolds number turbulence.

Full details of the ideas discussed here are given in the
references.

2. A TRANSITIONAL INSTABILITY

The processes by which laminar flows undergo transition to tur-
bulence remain basically unsolved. However, recent numerical studies
have provided some insights into transition, including:

(1) Non-classical character of transitional instabilities --
The primary linear (exponential) instability of classical plane
parallel shear flows with non-inflectional velocity profiles, as
described by the Orr-Sommerfeld (or related) equations, is much too
weak to describe transition. For example, linear instability of
plane Poiseuille flow (U(z) = 1 - z^2, |z| < 1) occurs for Reynolds

ties have been found in boundary layers, plane Couette flow, and pipe Poiseuille flow (see Orszag & Patera 1983) and in free shear flows (see Brachet & Orszag 1983).

(iv) Competition between two-dimensional pairing and three-dimensional instabilities -- Inflectional (free shear) flows, like mixing layers and jets, are inviscidly unstable to two-dimensional disturbances. Squire's theorem implies that these instabilities are strongest when two-dimensional; when these two dimensional instabilities evolve in time they saturate into ordered laminar flow states characterized by large-scale vortical flow structures. These vortical flows may themselves be unstable to subharmonic (pairing) instabilities, in which two (or more) vortices are paired and generate a new larger-scale vortex motion (Patnaik, Sherman & Corcos 1976). In these flows, the three-dimensional instability discussed above may also be present (Pierrehumbert & Widnall 1982), but it is not necessarily stronger than the pairing instability. However, the three-dimensional secondary instability is effective at much smaller spanwise spatial scales than is the inviscid primary instability and seems to lead directly to chaotic flows (Brachet & Orszag 1983).

(v) 'Spurious (numerical) turbulence' -- Curry et al (1984) show that, while low-order dynamical systems derived by Galerkin approximation to the two-dimensional Boussinesq equations may exhibit chaotic solutions, this chaos typically disappears as the dimension of the projection space increases (see Figure 4). Similarly, it was shown by Orszag & Kells (1980) that under-resolved numerical calculations of transitional planar shear flows may be spuriously chaotic. Under-resolved computations do not have degrees of freedom associated with small spatial scales available to act as an eddy viscosity on well-resolved large-scales.
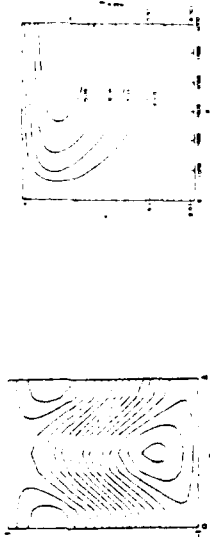

Figure 1. Streamlines of the steady (stable) finite-amplitude two-dimensional travelling wave for plane Poiseuille flow at R=4000, plotted in the rest frame of the wave. (from Orszag & Patera 1983).

Figure 2. Contours of constant growth rate (labelled by growth rate) as a function of R and the amplitude of the background two-dimensional nonlinear wave (see right-hand scale).

---

numbers $R_c > 5772$, while Squire's theorem implies that the critical disturbance is two-dimensional. The fact that this instability is induced by a subtle interplay of viscosity and shear implies that its growth rates are quite small on convective time scales. For example, the most rapidly growing exponential mode of the Orr-Sommerfeld equation is obtained at $R = 48,000$; its growth rate is only 0.0076; it is so feeble that perturbations grow by a factor 10 in a time of about 300, in which time a point on the centerline moves about 150 channel widths. In contrast, transition is observed to occur explosively over a few channel widths at Reynolds numbers as low as roughly 1000. A transitional instability that affects non-inflectional plane parallel shear flows must have a characteristic convective time scale.

(ii) Three dimensionality of transition -- Two-dimensional fluids do not appear to exhibit the kind of strong chaos that is characteristic of turbulent shear flows. In thermal convection, Curry et al (1983) show that two-dimensional flows do not appear to act in a strongly chaotic way, but three-dimensional flows may be strongly chaotic at large enough Reynolds number. Even for inflectional free shear flows, in which there are strong inviscid two-dimensional instabilities, Brachet & Orszag (1983) show that the flows that develop from two-dimensional finite-amplitude disturbances are not strongly chaotic, in contrast to the flows that develop three-dimensionally.

(iii) Instability of two-dimensional nonlinear travelling waves -- Perhaps the simplest instability that has the character of a transitional instability is the linear three-dimensional instability of two-dimensional finite-amplitude flows. Orszag & Kells (1980) show how such an instability fits the basic features of transition in classical shear flows, including their convective growth rates, inherent three-dimensionality, onset at Reynolds numbers in accord with experimental observations, and flow features in accord with early transitional flows. These instabilities have been analyzed both by direct numerical simulation of the evolving three-dimensional flow and by a linear perturbation analysis of the non-parallel two-dimensional (nonlinear travelling wave) flow. In Figure 1, we show the streamlines of a typical two-dimensional base state (here for plane Poiseuille flow at R = 4000). The non-parallel character of the base flow leads to considerable complication in its linear stability analysis; see Orszag & Patera (1983) for the formulation of these large matrix eigenvalue problems. A topic of much current research interest is the development of efficient numerical methods for finding eigenvalues of the very large matrices encountered in problems of this sort. In Figure 2, we give a stability diagram for this transitional instability; here we plot contours of constant growth rate as a function of the amplitude of the two-dimensional base state and the Reynolds number. The growth rates of this instability are 1-2 orders of magnitude larger than those of Orr-Sommerfeld modes. The development of this three-dimensional secondary instability seems to be consistent with available experimental data on early transitional flows. In Figure 3, we compare contours of the x-velocity at the so-called one-spike stage of transition in plane Poiseuille flow obtained (a) experimentally by Nishioka, Iida & Kanbayashi (1978) and (b) numerically by Kleiser & Schumann (1983). The flows that develop from the initial linear instability appear to lead directly to chaos and turbulence and not to saturate into ordered, laminar flow states. Similar instabili-

3. COMPUTER SIMULATIONS OF TURBULENCE

In this Section, I shall give three examples of numerical simulations of turbulent flows. The first two examples, turbulent channel flow and the simulation of a turbulent spot, are of the nature of numerical experiments in which the numericist uses the computer in much the same way as the experimentalist uses the laboratory, namely as a source of data about flows in a controlled environment. The final example, the Taylor-Green vortex, is an example in which the computer is being used to try to uncover fundamental physical laws of turbulence.

(i) Turbulent channel flow -- Turbulent channel flows have been simulated numerically three ways: (a) large-eddy simulation with a sub-grid-scale turbulence closure for eddies outside the wall layer and a heuristic boundary condition applied at the edge of the viscous sublayer by Deardorff (1970) and Schumann (1975); (b) large-eddy simulation with a sub-grid-scale turbulence closure applied to eddies of all scales including those in the wall layer by Moin & Kim (1982); and (c) full numerical solution of the Navier-Stokes equations by Orszag & Patera (1981). The really crucial differences are, as we shall see in Sec. 4 below, between (a) and (b-c). Simulations of type (a) have much smaller computational requirements at a given Reynolds number R than either of types (b) or (c), the latter requiring asymptotically similar computational work at large R. The deficiency of simulations of type (a) is that they require modelling of wall-layer effects in terms of an oversimplified boundary condition; the deficiency of types (b) and (c) is that, with currently available computer resolution (say 64 x 64 x 65 on a Cray-1 computer), Reynolds numbers are limited to about 10,000 (type b) or 5,000 (type a). For simulations of types b or c, the computational work scales as R³, so future increases in computer power do little to increase the effective Reynolds number of the computations.

Nevertheless, it is possible to achieve interesting results with full numerical solutions of the Navier-Stokes equations. In Figure 5, we plot the mean velocity profile found in the channel flow computations of Orszag & Patera (1981). The fit to a logarithmic wall layer velocity profile is only marginal, but the resulting von Karman constant 0.45 is within experimental bounds, so this calculation does give the first computation of a wall layer from the basic principles of fluid dynamics. Another more recent result from computations of this type is given in Figure 6, in which we plot the wall pressure spectrum in a moderate-resolution (32 x 32 x 33) run compared with available experimental data (see Handler et al 1983).

Figure 6. A plot of the turbulent wall pressure spectrum as a function of frequency (from Handler et al 1983).

Figure 3. Contours of x-velocity in the x-y plane at the one-spike stage in the laboratory experiments of Nishioka et al (top) and in the numerical simulation of Kleiser & Schumann (bottom). [From Kleiser & Schumann 1983.]

Figure 4. Time evolution of the Fourier component bq₂ of the temperature field in two-dimensional Benard convection at Ra = 120 Ra, Pr = 20 (Curry et al 1983). The numbers labelling each plot give the wavenumber cutoff used to derive the Galerkin approximation to the Boussinesq equations. Thus 1 x 2 gives the Lorenz equations, while the higher order models are higher order Galerkin approximations. Observe that as the resolution increases the chaos disappears.
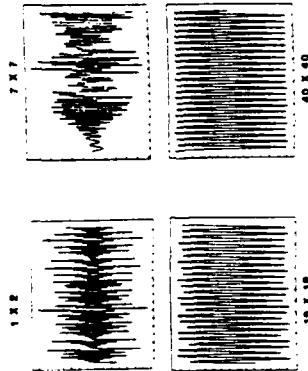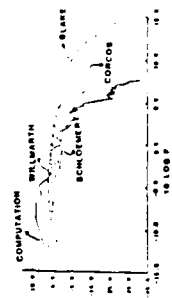

Figure 5. Mean turbulent profile obtained by full numerical simulation of plane Poiseuille flow at R = 5000 using a 64 x 64 x 65 spectral simulation. Note the viscous sublayer, buffer region, and logarithmic layer of 8-9 data points (from Orszag & Patera 1981).

(iii) Taylor-Green vortex -- In order to gain understanding of the basic physics of the generation of small-scale turbulent flow features, a nice model problem is the Taylor-Green (TG) vortex flow (Taylor & Green 1937; Brachet et al 1983). Here the flow is the which develops in time from initial conditions that consist of excitation in basically a single Fourier mode. Because of nonlinear interaction, the flow becomes strongly three-dimensional and develops excitation at all spatial scales. The TG vortex has been used to study such fundamental questions as the enhancement of vorticity by vortex-line stretching, the approach to isotropy of the small scales, possible singular behavior of the Euler equations, formation of an inertial range, and analysis of the geometry, and intermittency, of high-vorticity regions. The TG flow is advantageous for these studies because its special symmetries has allowed the development of numerical algorithms that are a factor 64 more efficient in both memory and storage than conventional periodic-geometry spectral methods. For a three-dimensional flow, this factor 64 translates into a factor 4 increased range of spatial scales -- it is now possible to compute the TG vortex flow with 512 x 512 x 512 Fourier modes for each velocity component on the Cray-1 computer (or more than 4 x 10^8 effective degrees of freedom).

One of the more exciting results to emerge from our studies of the TG flow is the suggestion that viscosity may play an essential role in the development of small-scale turbulence, not just acting as a sink of turbulent kinetic energy. Indeed, we find that the development of the turbulent flow seems to require viscosity to induce instabilities of vortical structures in which the initial large-scale non-turbulent vorticity undergoes an explosive redistribution in space (see Figure 9). These viscosity-induced instabilities are probably effective because viscosity allows vortex-line re-connections prohibited in inviscid flow. Similar diffusional instabilities have now been shown to be responsible for the generation of small-scale structures in two-dimensional magnetohydrodynamic (Frisch et al 1983) and kinetic (Brachet 1981) turbulence. Further study of viscosity-induced instabilities should clarify the development of intermittent flow structures in turbulence.
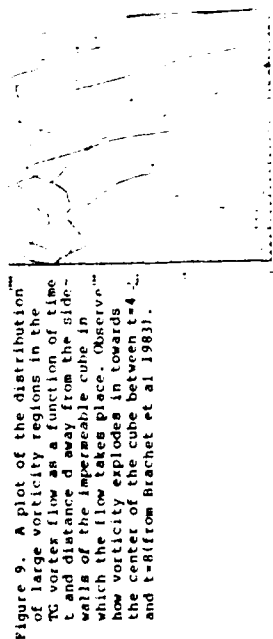
Figure 9. A plot of the distribution of large vorticity regions in the TG vortex flow as a function of time t and distance d away from the side-walls of the impermeable cube in which the flow takes place. Observe how vorticity explodes in towards the center of the cube between t=4 and t=8 (from Brachet et al 1983).

Despite the moderately low Reynolds number (R = 5000) of the simulation, agreement is achieved because flow features that do not depend explicitly on the boundary wall-layer structure tend to be Reynolds number independent.

(ii) Turbulent spot -- There has been much recent interest in the evolution of localized 'spots' in turbulent flows (see Wygnanski et al 1976). The first numerical simulation of a turbulent spot was reported by Leonard (1980), who used three-dimensional vortex filament techniques to compute the (inviscid) flow. More recently, we have begun a study of spots using full numerical solutions of the Navier-Stokes equations at moderate Reynolds numbers (Bullister & Orszag 1983). The latter simulations are performed by forcing the initial flow using a localized force to drive a jet of fluid vertically, then allowing the disturbance to evolve naturally. In Figures 7 and 8, we plot contours of maximum vertical z-velocity in the x-y and x-z planes at various times of evolution of plane Poiseuille flow. The character of this spot evolution is similar to that observed experimentally: the spot seems to spread in the spanwise direction by "transverse contamination", in agreement with the dye injection experiments of Gad-el-Hak et al (1981); the greatest turbulent activity is near the edges of the spot; the 'spreading' angle of the spot relative to its source is about 10°, in agreement with the channel flow experiments of Carlson et al (1982); the vertical structure of the spot is in qualitative agreement with that observed experimentally. Further numerical experiments are underway that should elucidate details of the flow in spots and the surrounding fluid.
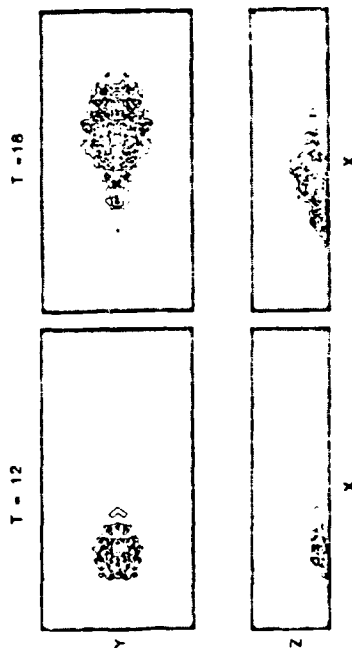

Figure 7. Contours of the maximum z-velocity in the x-y plane at t=12, 18 after initializing a turbulent spot computation by imposed vertical forcing. These computations are performed using a spectral code with 128(x) x 32(y) x 32(z) resolution. Fourier series are used in x and y; Chebyshev polynomial expansions are used in z.

Figure 8. Same as Figure 7, except x-z contours of max$_{x,y}|v_z|$. Here R = 6000.

4. SUB-GRID-SCALE TURBULENCE CLOSURES

Perhaps the most distinguishing characteristic of high Reynolds number turbulent flows is their large range of excited space and time scales. In homogeneous turbulence, dissipation-scale eddies are of order $R^{3/4}$ times smaller than energy-containing eddies. Including the effect of this range of spatial scales on the allowable time step in a numerical solution of the Navier-Stokes equations gives the estimate that order R^3 operations are required to simulate a turbulent flow. This is the reason for interest in the large-eddy-simulation method in which excitations on scales smaller than those resolvable numerically are modelled, usually by an eddy viscosity coefficient (see Deardorff 1970, Schumann 1975). The basic action of an eddy viscosity on large eddies is reasonable, although it cannot reproduce the random character of the action of small-scale eddies. However, in order to model properly wall turbulence, it is necessary to extend the sub-grid modelling ideas of Deardorff and Schumann and treat the turbulence all the way up to a rigid wall, as in recent work by Moin & Kim (1982). Unfortunately, in order for Moin & Kim to resolve motions down to the scale of turbulent bursts, which is necessary in order to capture the mechanism producing the turbulence, the work restriction O(R) remains. Thus, the Reynolds number restrictions are similar on large-eddy and full numerical solutions of the Navier-Stokes equations that attempt to integrate all the way through the wall layer region.

In recent work, Yakhot & Orszag (1983) have used dynamic renormalization group (RNG) methods to treat wall-bounded turbulence. The idea of the infrared RNG method is to use perturbation methods based on the direct-interaction approximation (Kraichnan 1959) to eliminate all small spatial scales up to the resolvable grid-scale from the Navier-Stokes equations. This is done perturbatively by eliminating narrow bands of wavevectors from the dynamics (see Figure 10), renormalizing the resulting reduced dynamical equation to have the form of the Navier-Stokes equations with modified viscosity and random forcing terms, and then repeating the process iteratively until all the required small scales are removed. The resulting dynamical equations involve a modified eddy viscosity and a random force, both induced by renormalization. The eddy viscosity is modified from the Smagorinsky viscosity used by Deardorff, Schumann, and

$$0 \qquad k_0 \qquad k \qquad \Lambda e^{-l} \qquad \Lambda$$

Figure 10. A schematic representation of the modal structure of the dynamic renormalization group. Here k_0 represents wavenumbers within the energy containing range, while Λ gives the high wavenumber (viscous) cutoff. Modes in the cross-hatched band are removed at each step of the RNG procedure.

Moin & Kim in the wall regions in which there is interference between the eddy and molecular viscosities. This interference effect is the key to obtaining a faithful representation of the wall region. Also, the induced random force is large in the buffer layer between the viscous sublayer and the logarithmic layer, giving a turbulence source in this region. Further work is now underway applying these RNG-based closures to both large-eddy simulations of turbulent shear flows and to the derivation of new classes of turbulence transport (Reynolds averaged) equations that should be useful in engineering applications.

5. CONCLUSIONS

I have reviewed several areas of activity in the numerical simulation of transition and turbulence in which I have been intimately involved recently. In this short space, it has not been possible to do justice to all of the large number of researchers involved in these fields; the references do a more complete job of surveying the literature. The principal conclusions from our studies are:

(i) Numerical methods now provide essential information complimentary to that available from experiment and mathematical analysis.

(ii) Computational fluid mechanics has now matured so that there are techniques that can be reliably applied to the most difficult of fluid mechanical problems. In contrast to 10 years ago, it is no longer mainly a question of how to compute a complicated flow; rather, now it is a question of which flow to compute in order to extract the most useful information.

(iii) It is crucial, especially in our studies of transitional flows, that we have used spectral numerical methods (see Gottlieb et al 1983 for a recent review). Spectral methods are so accurate for these problems that we can confidently conclude that properly tested numerical results are true fluid mechanical results. In contrast to finite difference or finite element methods in which an increase in spatial resolution by a factor 2 leads to an error decrease by a factor 4 or 8 or so, with spectral methods a factor 2 increase in resolution typically decreases the error by several orders of magnitude. This permits accurate verification of results. For example, in recent studies of transition in circular Couette flow, Marcus et al (1982) and Marcus (1983) have been able to achieve at least three-decimal-place agreement with experiment on wave speeds. The confidence in these results has permitted new analytical insights into the character of the onset of wavy instabilities of Taylor vortices in Couette flow (Bayly & Marcus 1983).

(iv) New generations of bigger and faster computers can most profitably be used to extend the range of application of computational fluid dynamics. Transition and turbulence problems in complex geometries with complex physics, like multi-phase flows, will surely be the subject of studies in the near future.

REFERENCES

Bayly, B. J. & Marcus, P. S. 1983 Analytic computation of Taylor-Couette wave speeds. To be published.

Brachet, M. E. 1983 To be published.

Brachet, M. E., Meiron, D. I., Orszag, S. A., Nickel, B. G., Morf, R. H. & Frisch, U. 1983 Small-scale structure of the Taylor-Green vortex. J. Fluid Mech. 130, 411-452.

Brachet, M. E. & Orszag, S. A. 1983 Secondary instability of free-shear flows. Submitted to J. Fluid Mech.

Bullister, E. T. & Orszag, S. A. 1983 Numerical simulation of turbulent spots. To be published.

Carlson, D. R., Widnall, S. E. & Peeters, M. F. 1982 A flow-visualization study of transition in plane Poiseuille flow. J. Fluid Mech. 121, 407-505.

Curry, J. H., Herring, J. R., Loncaric, J. & Orszag, S. A. 1983 Order and disorder in two- and three-dimensional Benard convection. Submitted to J. Fluid Mech.

Deardorff, J. W. 1970 A numerical study of three-dimensional turbulent channel flow at large Reynolds numbers. J. Fluid Mech. 41, 453-480.

Frisch, U., Pouquet, A., Sulem, P.-L. & Meneguzzi, U. 1983 To be published.

Gad-el-Hak, M., Blackwelder, R. F. & Riley, J. J. 1981 On the growth of turbulent regions in laminar boundary layers. J. Fluid Mech. 110, 73-95.

Gottlieb, D., Hussaini, M. Y. & Orszag, S. A. 1983 Theory and applications of spectral methods. In Proc. Symp. on Spectral Methods. SIAM, Philadelphia, to appear.

Handler, R. A., Hanson, R. J., Sakell, L., Bullister, E. T. & Orszag, S. A. 1983 Calculation of the wall-pressure field in a turbulent channel flow. Submitted to Phys. Fluids.

Kleiser, L. & Schumann, U. 1983 Laminar-turbulent transition process in plane Poiseuille flow. In Proc. Symp. on Spectral Methods. SIAM, Philadelphia, to appear.

Kraichnan, R. H. 1959 The structure of isotropic turbulence at very high Reynolds numbers. J. Fluid Mech. 5, 497-543.

Leonard, A. 1980 Vortex simulation of three-dimensional, spotlike disturbances in a laminar boundary layer. In Turbulent Shear Flows II, ed. by L. J. S. Bradbury et al, Springer, pp. 67-77.

Marcus, P. S. 1983 To be published.

Marcus, P. S., Orszag, S. A. & Patera, A. T. 1982 Simulation of circular Couette flow. In Proc. Eighth Intl. Conf. on Numerical Methods in Fluid Dynamics, ed. by E. Krause, Springer, pp. 371-376.

Moin, P. & Kim, J. 1982 Numerical investigation of turbulent channel flow. J. Fluid Mech. 118, 341-377.

Nishioka, M., Iida, S. & Kanbayashi, S. 1978 An experimental investigation of the subcritical instability in plane Poiseuille flow. In Proc. 10th Turbulence Symposium, Inst.

Space Aero. Sci., Tokyo Univ., pp. 55-62.

Orszag, S. A. & Kells, L. C. 1980 Transition to turbulence in plane Poiseuille and plane Couette flow. J. Fluid Mech. 96, 159-205.

Orszag, S. A. & Patera, A. T. 1981 Calculation of von Karman's constant for turbulent channel flow. Phys. Rev. Letters 47, 832-835.

Orszag, S. A. & Patera, A. T. 1983 Secondary instability of wall-bounded shear flows. J. Fluid Mech. 128, 347-385.

Patnaik, P. C., Sherman, F. S. & Corcos, G. M. 1976 A numerical simulation of Kelvin-Helmholtz waves of finite amplitude. J. Fluid Mech. 73, 215-240.

Pierrehumbert, R. T. & Widnall, S. E. 1982 The two- and three-dimensional instabilities of a spatially periodic shear layer. J. Fluid Mech. 114, 59-82.

Schumann, U. 1975 Subgrid scale model for finite difference simulations of turbulent flows in plane channels and annuli. J. Comp. Phys. 18, 376-404.

Taylor, G. I. & Green, A. E. 1937 Mechanism of the production of small eddies from large ones. Proc. Roy. Soc. A158, 499-521.

Wygnanski, I. J., Sokolov, M. & Friedman, D. 1976 On a turbulent 'spot' in a laminar boundary layer. J. Fluid Mech. 78, 785-819.

Yakhot, V. & Orszag, S. A. 1983 Renormalization group formulation of large eddy simulation. Submitted to J. Fluid Mech.

53) A.T. PATERA: A spectral element method for fluid dynamics: laminar flow in a channel expansion. J. Comp. Phys. 54, 468-488 (1984).

54) PROCEEDINGS of the Second IUTAM Conference on Laminar-Turbulent Transition, Novosibirsk, July 9-13, 1984. To be published by Springer-Verlag.

55) R.S. ROGALLO, P. MOIN: Numerical simulation of turbulent flows. Ann. Rev. Fluid Mech. 16, 99-137 (1984).

56) W.S. SARIC, A.S.W. THOMAS: Experiments on the subharmonic route to turbulence in boundary layers. Proc. IUTAM Symposium "Turbulence and Chaotic Phenomena in Fluids", Kyoto, Japan (1983).

57) W.S. SARIC, V.V. KOZLOV, V.Y. LEVCHENKO: Forced and unforced subharmonic resonance in boundary layer transition. AIAA paper No. 84-0007 (1984).

58) K.R. SREENIVASAN: Transitional and turbulent wakes and chaotic dynamical systems. This volume.

59) J.T. STUART: On the non-linear mechanics of hydrodynamic stability. J. Fluid Mech. 4, 1-21 (1958).

60) I. TANI: Boundary-layer transition. Ann. Rev. Fluid Mech. 1, 169-196 (1969).

61) T. TATSUMI (ed.): Proc. IUTAM Symposium on Turbulence and Chaotic Phenomena in Fluids. Sept. 5-10, 1984, Kyoto.

62) R.G. VOIGT et al. (ed.): Spectral methods for partial differential equations. SIAM, Philadelphia (1984).

63) D.R. WILLIAMS, H. FASEL, F.R. HAMA: Experimental determination of the three-dimensional vorticity field in the boundary layer transition process. To appear in J. Fluid Mech.

64) F.X. WORTMANN: The incompressible fluid motion downstream of twodimensional Tollmien-Schlichting waves. AGARD-CP-224, 12-1 - 12-8 (1977).

65) A. WRAY, M.Y. HUSSAINI: Numerical experiments in boundary-layer stability. AIAA Paper 80-0275 (1980).

66) J.P. ZAHN, J. TOOMRE, E.A. SPIEGEL, D.O. GOUGH: Nonlinear cellular motions in Poiseuille channel flow. J. Fluid Mech. 64, 319-345 (1974).

RENORMALIZATION GROUP FORMULATION OF LARGE EDDY SIMULATION

V. YAKHOT, S.A. ORSZAG

1. INTRODUCTION

Perhaps the most distinguishing characteristic of high Reynolds number turbulent flows is their large range of excited space and time scales. I... homogeneous turbulence, dissipation-scale eddies are of order $R^{3/4}$ time... smaller than energy-containing eddies, where R is the Reynolds number. I... order to solve the Navier-Stokes equations accurately for such a turbulen... flow, it is necessary to retain order $(R^{3/4})^3$ spatial degrees of freedom Also, since the time scale for significant evolution of homogeneous turbu... lence is of the order of the turnover time of an energy containing eddy, i... is necessary to perform order $R^{3/4}$ time steps to calculate for a signif... icant evolution time of the flow. Even if these calculations require onl... 0(1) arithmetic operations per degree of freedom per time step, the tota... computational work involved would be order R^3, while the computer storag... requirement would be $R^{9/4}$. In this case, doubling the Reynolds numbe... would require an order of magnitude improvement in computer capability... With this kind of operation and storage count, it is unlikely that forsee... able advances in computers will allow the full numerical simulation c... turbulent flows at Reynolds numbers much larger than $R_\lambda = 0(100)$ alread... achieved (see BRACHET et al. [21]).

This pessimistic operation and storage count for solution of t... Navier-Stokes equation is the origin of interest in the so-calle... large-eddy-simulation method. Here, excitations on scales smaller th... those resolvable on the numerical grid are modelled, usually by an edd... viscosity coefficient. Such a subgrid scale (SGS) eddy coefficien... represents the dissipative effect of motions on scales smaller than t... effective grid on the large eddies (defined as those motions adequatel... represented on the numerical grid). The most common form for this SGS edd... viscosity coefficient is due to SMAGORINSKY

$$\nu_{eddy} = c\Delta^2 \left[\left[\frac{\partial v_i}{\partial x_j} + \frac{\partial v_j}{\partial x_i}\right]^2\right]^{1/2}$$

(1.

where Δ is the grid scale and v_1 is the large-eddy velocity. It has been shown by LILLY [12] that the eddy viscosity (1.1) is consistent on dimensional grounds with the Kolmogorov theory of the inertial range. For the inertial-range spectrum $E(k) = C_ε^{2/3}k^{-5/3}$ with $C = 1.5$, LILLY argued that $c ≈ 0.04$ in (1.1).

The basic action of the eddy viscosity (1.1) on large scales seems correct in most respects. However, there are two important qualitative deficiencies in this formulation of large-eddy simulations. First, large-eddy simulations based on (1.1) alone neglect the effect of random forcing of small scales at the subgrid level on large scales at the supergrid level. The eddy viscosity (1.1) is non-stochastic (at the subgrid level, though it is still random due to supergrid fluctuations), while the action of random small-scale eddies is certainly stochastic in character. Thus, it should be expected that in addition to eddy viscous effects of small scales on large scales, there should also be a random forcing effect, giving rise to an eddy diffusion process and production of turbulent energy. This point will be discussed later. Second, the eddy viscosity (1.1) does not properly model interference effects between eddy and molecular viscosity, which is essential in turbulent processes where eddy effects must be inhibited (for example, near rigid walls). The simple superposition of eddy and molecular viscosity near rigid walls does not lead to correct results (see MOIN & KIM [14]).

DEARDORFF [4,6,7] made pioneering studies of turbulent shear flows using the SGS viscosity (1.1). For wall-bounded shear flows, DEARDORFF calculated only up to the edge of the buffer layer between the viscous sublayer and the logarithmic region of the velocity profile. A boundary condition is imposed at this point, based on the von Karman theory of the wall layer, in which the turbulent fluctuating stress is assumed known. Molecular viscosity plays no role in DEARDORFF's calculations, which are performed at cast formally, at infinite R. Clearly such a simulation does not give a faithful representation of the wall region and accompanying bursts.

If one is interested in the physics of wall turbulence, neglect of the wall region is unjustified. More recent work by MOIN & KIM [14] integrates up to the rigid wall, the increased sophistication giving a so-called transport-eddy simulation. However, transport-eddy simulations (as currently implemented) are much more severely limited than the earlier large-eddy simulation work of DEARDORFF and SCHUMANN. The point is that, presently practiced, transport-eddy subgrid scale simulations use uniform horizontal resolution independent of distance from the wall (MOIN & KIM [14]). If such a simulation is to capture scales down to those of turbulent bursts (which must be done to capture the turbulence product properly), the number of required degrees of freedom scales as $R_λ^3$. This estimate is based on the fact that, while the streak structure scales with inner variables (KLINE et al. [10]), streamwise and spanwise corre-

lations scale with the outer variables, i.e. channel height (COMTE-BELL [3]). Transport-eddy modelling does allow simulation of flows at somewhat higher Reynolds numbers than those that can be simulated without modelling (MOIN & KIM [14] achieve $R_λ = 640$ ($R = = 13000$) by transport-eddy modelling, while the direct numerical simulations of ORSZAG & PATERA [] are restricted to $R_λ = 200$), but bursts at mean-flow Reynolds numbers R 20000 - 100000 (in plane Poiseuille flow) are beyond subgrid scale modelling as now implemented in Cray-1 class computers. In other words, if a transport-eddy simulation of a well-bounded flow is to fare significantly better than a direct simulation, the dependence of required degrees freedom must scale less rapidly than $R_λ^3$ as $R_λ$ becomes large. At present no such method exists.

A second problem with current transport-eddy schemes stems from the way the small scales are modelled in the wall layer. In particular, the application of a VAN DRIEST correction to the subgrid eddy viscosities (MOIN & KIM [14]) is not fully justified. While this correction (VAN DRIEST [17]) was originally intended to model the effect of fluctuations within the viscous sublayer in modulating the interaction of molecular and eddy viscosities, applying it to a subgrid scale model could eliminate significantly alter fluctuations in the supergrid or resolvable scales. A third problem is that existing schemes rely upon availability of experimental data to fix modelling constants. For example, MOIN & KIM [] introduce a new term into the equation of motion to obtain the correct mean velocity profile in turbulent channel flow. To achieve agreement with experiment, they chose parameters that differ from those that seem work best for homogeneous turbulence. Other choices of parameters give unrealistic turbulence decay or growth.

In this paper, we use renormalization group (RNG) methods to address solution of the latter two difficulties encountered by transport-eddy modelling. The RNG SGS closures obtained below seem to model properly interaction of turbulent motions in the wall region without ad hoc damping factors, and also appear to account for the generation of random bursts in the buffer layer, without requiring extensive experimental data to fix transport coefficients. The problem of computational work scaling as $R_λ^3$ will be addressed once again in the conclusion of this paper, but remains subject of current investigation.

2. INFRARED RNG METHOD FOR HOMOGENEOUS TURBULENCE

FORSTER, NELSON & STEPHEN [8] introduced the infrared RNG method to investigate the long-time-large-scale properties of randomly stirred fluid. Their work, as well as the subsequent work of MARTIN & DE DOMINICIS, []

FOURNIER & FRISCH [9], and YAKHOT [19], showed that the large-scale spectrum of an incompressible fluid governed by the Navier-Stokes equations subject to a Gaussian random force that is white in time and with energy spectrum proportional to k^{-3} (see (2.2) below), generates the Kolmogorov $k^{-5/3}$ energy spectrum in the infrared ($k \to 0$) limit.

The problem treated by the above authors is:

$$\frac{\partial \vec{v}}{\partial t} + \vec{v} \cdot \nabla \vec{v} = -\frac{\nabla P}{\rho} + \vec{f} + v_0 \nabla^2 \vec{v}; \qquad (2.1a)$$

$$\nabla \cdot \vec{v} = 0 \qquad (2.1b)$$

with

$$\langle f_j(\vec{k}, \omega) f_j(\vec{k}', \omega') \rangle = 2(2\pi)^4 D_0 k^{-3} \left[\delta_{ij} - \frac{k_i k_j}{k^2} \right] \delta(\vec{k}+\vec{k}') \delta(\omega+\omega') \qquad (2.2)$$

In this section, we rework the infrared RNG method for the problem (2.1) - (2.2) in order to demonstrate how RNG ideas may fit into the context of subgrid scale closure. However, before proceeding to this task let us give some further justification for the inclusion of the random force (2.2) as a driving force in the Navier-Stokes equations (2.1).

On the one hand, the random force (2.2) is justified by earlier work on the infrared renormalization group because of its consistency with the $k^{-5/3}$ spectrum at small k. However, for our present purposes this is but weak justification, because we are interested in eliminating only the very smallest scales (highest k) of motion that represent the SGS motions. YAKHOT [19] generalized the RNG methods to the ultraviolet case, in which the largest scales of motion are removed by the RNG procedure, and showed that a high-wave number $k^{-5/3}$-like spectrum is also achieved by imposing the random force (2.2). Also, YAKHOT [19] showed that if a field of homogeneous turbulence is driven by a force confined by a band of wave numbers, then the ultraviolet RNG procedure induces a random force at high wave numbers of the form (2.2). The assumptions leading to the latter conclusions have recently been weakened (YAKHOT, unpublished). In any case, if it is to be assumed that the smallest scales of turbulence are governed by KOLMOGOROV-like laws, then we conclude that it is consistent to include the random driving force (2.2) in the equations of motion for the small scales.

The idea of the infrared RNG method is to eliminate modes from the wavenumber strip near the ultraviolet cutoff Λ. Modes in the band $\Lambda e^{-\ell} < k < \Lambda$ are formally removed, using diagrammatic perturbation theory, the latter being structurally similar to that introduced for homogeneous turbulence theory by KRAICHNAN [11] and WYLD [18]. The system resulting from the

elimination of these modes involves modified interaction coefficients, new nonlinearities, as well as modified viscosities and forces. In the method, the resulting equations are then transformed to look as much possible like the original system (2.1) - (2.2).

To illustrate the technical details of the RNG method, consider Fourier transform of (2.1):

$$v_\ell(\hat{k}) = G^0 f_\ell(\hat{k}) - \frac{i\lambda_0}{2} G^0 P_{\ell mn}(\hat{k}) / v_m(\hat{q}) v_n(\hat{k}-\hat{q}) d\hat{q}$$

where $\hat{k} = (\vec{k}, \omega)$ and

$$G^0 = (-i\omega + v_0 k^2)^{-1}; \qquad P_{\ell mn}(\hat{k}) = k_m P_{\ell n}(\hat{k}) + k_n P_{\ell m}(\hat{k}) ;$$

$$P_{\ell m}(\hat{k}) = \delta_{\ell m} - \frac{k_\ell k_m}{k^2}$$

The integration on the right side of (2.3) is carried out over the domain $\hat{q} = (\vec{q}, \Omega)$ with $-\infty < \Omega < \infty$ and $0 < q < \Lambda$. At this stage, we are interested in the effect of the modes from the strip $\Lambda e^{-\ell} < k < \Lambda$. The velocity field is split into the two components: $v^<(\hat{k})$ with $0 < k < \Lambda e^{-\ell}$ and $v^>(\hat{k})$ with $\Lambda e^{-\ell} < k < \Lambda$. In terms of this decomposition, the integral in (2.3) becomes:

$$v_\ell(k) = G^0 f_\ell(k) + \frac{i\lambda_0}{2} G^0 P_{\ell mn}(\hat{k}) \times$$

$$\times \int [v^<_m(\hat{q}) v^<_n(\hat{k}-\hat{q}) + 2 v^<_m(\hat{q}) v^>_n(\hat{k}-\hat{q}) + v^>_m(\hat{q}) v^>_n(\hat{k}-\hat{q})] d\hat{q}$$

In order to eliminate modes from the interval $\Lambda e^{-\ell} < k < \Lambda$, all terms $v_\ell^>$ in (2.5) should be removed by repeated substitution of (2.5) for $v^>$ into (2.5). This generates an infinite expansion for $v^>$ in powers of $v^<$ which $v^>$ does not formally appear. Next, averages are taken over the modes of random force $f^>$ belonging to the strip $\Lambda e^{-\ell} < k < \Lambda$. This procedure formally eliminates the modes $\Lambda e^{-\ell} < k < \Lambda$ from the problem; the resulting terms represented diagrammatically in Fig. 1, where the thick slashed unmeshed lines symbolize modes $v^>(\hat{k})$ and $v^<(k)$, respectively. The thick slashed line denotes $2D_0 |G^0(\hat{k})|^2 P_{ij}(\hat{k}) k^{-3} \delta(\hat{k}+\hat{k}')$, while the vertex and $\cdots$ denote $-\frac{i\lambda_0}{2} P_{\ell mn}(\hat{k})$ and random force $f(\hat{k})$, respectively.

It follows from Fig. 1, that after removing the modes $\Lambda e^{-\ell} < k < \Lambda$, equation of motion for $v^<$ can be written up to second order in λ_0 as:

$$(-i\omega + v_0 k^2) v^<_\ell(\hat{k}) = f_\ell(\hat{k}) - \frac{i\lambda_0}{2} P_{\ell mn}(\hat{k}) / f^<_n(\hat{q}) v^<_m(\hat{k}-\hat{q}) d\hat{q} -$$

$$-\frac{1}{2}\lambda_0 P_{lmn}(k) \int v_m(q) v_n(k-q)\, dq +$$

$$\qquad(2.6)$$

$$+ 4D_0 \left(\frac{\lambda_0}{2}\right)^2 P_{lmn}(\vec{k}) \int |G^0(\vec{q})|^2 P_{m\mu}(\vec{q}) P_{n\mu\rho}(\vec{k}-\vec{q}) q^{-3} G^0(\vec{k}-\vec{q}) v^<_\rho(\vec{k})\, dq + O(\lambda_0^3)$$

The second term on the right side of (2.6) is an induced random force, denoted by Δf, with zero mean if the forces in modes k' are assumed to be statistically homogeneous.

When the $O(\lambda_0^2)$ term on the right-side of (2.6) is moved to the left side, it gives a correction to the bare viscosity $\nu_0 k^2$:

$$k^2 \Delta\nu P_{l,i}(k) =$$
$$= \lambda_0^2 D_0 P_{lmn}(\vec{k}) \int |G^0(\vec{q})|^2 P_{m\mu}(\vec{q}) P_{n\mu\rho}(\vec{k}-\vec{q}) q^{-3} G^0(\vec{k}-\vec{q})\, d\vec{q}$$
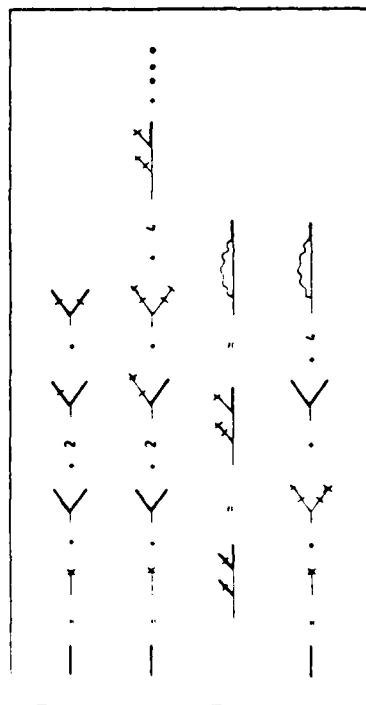
$$\qquad(2.7)$$

Fig. 1 A diagrammatic representation of the derivative of the renormalized Navier-Stokes equation (2.6).
(a) Diagrammatic representation of the Navier-Stokes equation (2.5).
(b) Irreducible diagram expansion of the equation for v' with v' removed.
(c) Second-order correction to propagator, included in (2.6).
(d) Renormalized Navier-Stokes equation (2.6), closed at second-order diagrams as in the quasi-normal approximation, which is asymptotically exact in the limit $t \to 0$.

The integration in (2.7) is carried out over $\vec{q} = (\vec{q},\Omega)$ where $-- < \Omega <$. $\Lambda e^{-t} < q < \Lambda$. Integration over the frequency Ω gives

$$k^2 \Delta\nu P_{l,i}(\vec{k}) = \frac{\lambda_0^2 D_0}{\nu_0} P_{lmn}(\vec{k}) k_\nu \int_{\Lambda e^{-t}}^{\Lambda} \frac{P_{m\mu}(\vec{q}) P_{n\mu\rho}(\vec{k}-\vec{q}) q^{-d-2}}{-t\omega + \nu_0 (q^2 + |k-q|^2)} \frac{d^d q}{(2\pi)^d}$$

$$\qquad(\;)$$

where we have now generalized the formula to d dimensions with k^{-3} in (2 replaced by k^{-d}.

The correction $\Delta\nu$ to the viscosity is a function of both ω and $\vec{k}$. Since we are interested in behaviour of the system at large scales, we neglect k in comparison and q and ω in comparison with $\nu_0 q^2$ in (2.8). This gives

$$\Delta\nu(\vec{0}) = \bar{A}_d \frac{\lambda_0^2 D_0}{\nu_0^2 \Lambda} \frac{e^{4t} - 1}{4}$$

$$\qquad(\;)$$

where

$$A_d = \bar{A}_d \frac{S_d}{(2\pi)^d}, \quad \bar{A}_d = \frac{1}{2} \frac{d^2-2}{d^2+2d}$$

$$\qquad(2\;)$$

where $S_d = 2\pi^{d/2}/\Gamma(d/2)$ is the area of a unit sphere in d dimensions. The the viscosity resulting from elimination of the modes ν' is:

$$\nu = \nu_0 (1 + \lambda_0^2 d \lambda_0^{-2} \frac{e^{4t}-1}{4})$$

$$\qquad(2\;)$$

where the dimensionless coupling constant $\bar{\lambda}_0$ is

$$\bar{\lambda}_0 = \lambda_0 \frac{D_0^{1/2}}{\nu_0^{3/2} \Lambda^{\frac{d}{2}}}$$

$$\qquad(2\;)$$

The elimination procedure just described is accurate in the limit $t \to 0$. conclude that elimination of small scales with $\Lambda e^{-t} < k < \Lambda$ affects neith λ_0 nor D_0. The constancy of D_0 under this renormalization foll because, while the second term on the right-hand side of equ. (2.6) give zero-mean (averaged over k') Gaussian random variable with correlat function proportional to k^2, this correction cannot be absorbed in bare force (2.2) whose correlation function is proportional to k^{-3}. Th $D = D_0$, and we must include a new random force with correlation funct proportional to k^2 in the renormalized Navier-Stokes equations. The f that λ_0 is not renormalized is a consequence of Galilean invariance (FORSTER et al. [8].

It is possible to eliminate a finite band of modes $\Lambda e^{-\ell} < k < \Lambda$ by iterating the above procedure of eliminating an infinitesimally narrow band of modes. The result of this iteration procedure is to generate a renormalized viscosity coefficient $\nu = \nu(\ell)$ and coupling constant $\bar{\lambda} = \bar{\lambda}(\ell)$, while $\nu(\ell) = D_0$ and $\lambda(\ell) = \lambda_0$ still hold. Whereas the elimination of the infinitesimal band of modes is justified by comparison with second-order perturbation solutions of the Navier-Stokes equations (or by comparing with the direct-interaction approximation for this system), the result of the iteration procedure is no longer justifiable in this way. The nature of the errors incurred by this procedure must be clarified later.

The functions $\nu(\ell)$ and $\bar{\lambda}(\ell)$ are most easily determined by taking the limit $\ell \to 0$ in (2.9) in order to obtain the differential equation

$$\frac{d\nu}{d\ell} = A_d \nu(\ell) \bar{\lambda}^2(\ell)$$ (2.13)

where

$$\bar{\lambda}^2(\ell) = \frac{\lambda_0^2 D_0}{\nu^3(\ell)} A_d e^{4\ell}$$ (2.14)

Since $\Lambda(\ell) = \Lambda e^{-\ell}$.

The solution of (2.13)-(2.14) is

$$\nu(\ell) = \nu_0 (1 + \frac{3}{4} A_d \bar{\lambda}_0^2 (e^{4\ell} - 1))^{1/3}$$ (2.15)

and

$$\bar{\lambda}(\ell) = \bar{\lambda}_0 e^{2\ell} (1 + \frac{3}{4} A_d \bar{\lambda}_0^2 (e^{4\ell} - 1))^{-1/2}$$ (2.16)

In the 'infrared' limit $\ell \to \infty$, the dimensionless coupling parameter $\bar{\lambda}$ approaches the finite limit

$$\bar{\lambda}^* = \sqrt{4/3 A_d}$$ (2.17)

Pretending that the coupling constant $\bar{\lambda} << 1$ at this "fixed point", so that the nonlinear terms of the renormalized Navier-Stokes equation become negligible as $\ell \to \infty$, we find that the renormalized velocity field is given by

$$v_i(k) = G_R(k) f_i(k)$$ (2.18)

where the renormalized propagator $G_R(k)$ is given by

$$G_R(k) = (-i\omega + \nu(\ell) k^2)^{-1}$$

If only modes with wavenumbers larger than $k = \Lambda(\ell)$ are removed by renormalization, then (2.15) gives the k-dependent viscosity:

$$\nu(k) = (\frac{3}{4} A_d D_0)^{1/3} k^{-4/3}$$

where we have now set $\lambda_0 = 1$. Noting (2.18), averaging over random force with correlation function k^{-3}, and integrating over ω gives one-dimensional energy spectrum $E(k)$:

$$E(k) = \frac{1}{2} \frac{S_d}{(2\pi)^d} \frac{1}{d+1} \int_{-\infty}^{\infty} G_i(k\omega) d\omega = \frac{1}{2(\frac{3}{8} A_d)^{1/3}} (2D_0)^{2/3} \frac{S_d}{(2\pi)^d} \bar{\lambda}^{2/3} k^{-5/3}$$

$$G_{ij}(k\omega) = \frac{<v_i(k\omega) v_j(k'\omega')>}{(2\pi)^{d+1} \delta(k+k')\delta(\omega+\omega')}$$

Formula (2.21) has also been derived by FOURNIER & FRISCH [9].

It follows from (2.18) that

$$2 \frac{S_d}{(2\pi)^d} D_0 \ell_n \frac{\Lambda(\ell)}{k_0} = \epsilon_R$$

where

$$\epsilon_R = \frac{1}{2} \nu(\ell) \left(\frac{\partial v_i}{\partial x_j} + \frac{\partial v_j}{\partial x_i} \right)^2$$

is the (renormalized) rate of energy dissipation per unit mass (see NOVIKOV [15]. Since $\Lambda(\ell) = k$, (2.22) implies that ϵ_R is a weak function of k.

$$\frac{\epsilon_R}{\ell n k/k_0} = 2 \frac{S_d}{(2\pi)^d} D_0$$

independent of k. Substituting (2.24) into (2.21) gives

$$\epsilon(k) = C_K \epsilon^{2/3} k^{-5/3} / (\ell n k/k_0)^{2/3}$$

where we identify $\bar{\epsilon} = \epsilon_R$ as the rate of energy dissipation and

$$C_K = \frac{1}{2}\left(\frac{1}{8}\bar{\lambda}_d\right)^{1/3} \approx 1.13 \quad (d=3) \quad (2.26)$$

Here $(ink/k_0)^{-2/3}$ is a correction to the Kolmogorov $k^{-5/3}$ spectrum caused by the random force (2.2); C_K is the Kolmogorov constant that agrees reasonably well with $C_K = 1.5$ observed experimentally. This result will be used in the next section, where we apply renormalization group ideas to derive a subgrid scale model for finite systems.

It can also be shown that a somewhat more realistic model whose stirring force satisfies:

$$\langle f_i(k)f_j(k')\rangle = F\left[\delta_{ij} - \frac{k_i k_j}{k^2}\right]k^{-d}\delta(k+k')\delta(\omega+\omega'), \quad k \gtrsim k_c \quad (2.27)$$

for any $k_c > L^{-1}$, also gives the Kolmogorov spectrum in the limit $k \to \infty$. This is easily understood, since all the terms originating from the strip $L < k < k_c$ are irrelevant in the limit $k \to \infty$. This result is the key to our treatment of finite systems in section 3. *In particular, we assume that a turbulent fluid in a finite system in which the flow is locally homogeneous, exhibits the Kolmogorov behaviour in the intermediate range $k_c < k < k_d$ and can be described by the Navier-Stokes equation (2.1) with the random force (2.27) locally in physical space.*

3. SUBGRID SCALE MODEL FOR INHOMOGENEOUS TURBULENCE

In this section, we describe the application of the infrared RNG method to the development of a subgrid scale closure for inhomogeneous turbulent flows in finite geometries, like pipes and channels. It is well-known experimentally that if the Reynolds number is sufficiently large, one can distinguish three spatial scales in such flows: (i) for wavenumbers $k \lesssim 1/L$ (where L is a scale defining the geometry of the flow), the energy spectrum is anisotropic and is not characterized in any universal statistical way; (ii) for wavenumbers satisfying $1/L \ll k < k_d \approx R^{3/4}L^{-1}$, the velocity fluctuations in the turbulent fluid are characterized roughly by the $k^{-5/3}$ spectrum, (iii) in the dissipation range, $k \gtrsim k_d$, the energy spectrum decreases rapidly.

The finite, inhomogeneous systems under discussion here differ from the homogeneous systems discussed in Sec. 2 in that, while it is possible to

drive finite systems by forces like (2.2) to achieve a $k^{-5/3}$ small-scale spectrum, the parameter D_0 characterizing the amplitude of this force is not a free parameter, but rather is determined by the driving mechanism and boundary conditions of the inhomogeneous turbulent flow. In the homogeneous systems under discussion in Sec. 2, D_0 is directly proportional to the energy dissipation rate $\bar{\epsilon}$, so $\bar{\epsilon}$ is determined by the random force, hence is not a renormalizable parameter.

However, in a finite system, the average dissipation $\bar{\epsilon}$ is a function of velocity field, boundary conditions, and external driving mechanism this case, $\bar{\epsilon}$ should be determined dynamically from the equations motion. The dissipative cutoff is no longer an independent parameter according to the Kolmogorov theory of small-scale turbulent motions,

$$\bar{\lambda}_0^2 = \frac{\bar{\epsilon}}{\nu_0 k_d^4}\left(\frac{2\pi}{S_d}\right)^d$$

is dimensionless and typically order 1 in magnitude. In other words, Navier-Stokes equation with forcing (2.27) is subject to initial and boundary conditions, an element not existing in conventional renormalization group methods applied to infinite systems.

In finite systems, the average rate of energy dissipation per unit mass is:

$$\bar{\epsilon} = \frac{1}{V}\frac{1}{T}\int \epsilon(x,t)d^3x\,dt$$

where

$$\epsilon(x,t) = \frac{\nu_0}{2}\left(\frac{\partial v_i}{\partial x_j}+\frac{\partial v_j}{\partial x_i}\right) = \nu_0\frac{\partial v_i}{\partial x_j}\left(\frac{\partial v_i}{\partial x_j}+\frac{\partial v_j}{\partial x_i}\right)$$

where $V = L^3$ and T characterizes the time scale for evolution of the flow. Equations (2.1), (2.27), (3.2), (3.3) with the imposed initial and boundary conditions represent a closed set of equations to which we apply dynamic renormalization group ideas outlined in Sec. 2.

To evaluate $\bar{\epsilon}$ given by (3.2), (3.3), we eliminate small scales from the following the technique of Sec. 2. After elimination of scales of size order $V^{1/3}$ and smaller, it is clear that we can neglect the variation of in the volume V so that

$$\bar{\epsilon} \approx \epsilon$$

re $c^<(x,t)$ is the inverse Fourier transform of

$$c(k) = v_0 \int [q_l(k-q)v_l v_j(q)v_j(k-q) + q_l v_l(k-q)(k-q)_j v_j(q)]d\hat{q}/(2\pi)^{d+1}$$ (3.5)

ter elimination of small scales.

e integral in (3.5) contains all modes from the domain $0 < k < \Lambda$. Our al is to evaluate the coarse-grained or renormalized expression for dis- pation which does not include the modes $\Lambda e^{-\ell} < k < \Lambda$. As in Sec. 2, we troduce the modes $v^>(k)$ and $v^<(k)$ belonging to the strip $\Lambda e^{-\ell} < k < \Lambda$ and $k < \Lambda e^{-\ell}$, respectively. Then the first term on the right side of (3.5) omes

$$'_1 = v_0 \int q_l(k-q)_l [v_j^<(q)v_j^<(k-q) +$$

$$+ 2v_j^<(q)v_j^>(k-q) + v_j^>(q)v_j^>(k-q)]d\hat{q}/(2\pi)^{d+1}$$ (3.6)

order to eliminate $v^>$ from (3.6), we substitute the formal solution of e equation of motion (2.5) recursively for $v^>$ in (3.6). This generates a turbation expansion for ϵ_1 in powers of ℓ_0. The resulting series is then eraged over the part of the random force belonging to the interval $\Lambda e^{-\ell} <$ $\Lambda e^{-\ell}$. In this manner we eliminate the modes $v^>$. The procedure is presented diagrammatic form by Fig. 2. In the renormalization of ϵ there are two ds of vertices: the solid circle stands for $v_0 q_\ell(k-q)_\ell$ while the open cle stands for $-(1\lambda_0/2)P_{lmn}(k)$. It follows that

$$'_1 = -4 v_0 \lambda_0^2 D_0 \int q_j(k-q)_j P_{lmn}(q) P_{luv}(k-q) G_0^0(q) G_0^0(k-q)$$

$$\times |G^0(q-\hat{q}_2)|^2 |\hat{q}-\hat{q}_2|^{-d} P_{\mu n}(q-\hat{q}_2) v_m(\hat{q}_2) \times$$

$$\times v_j(k-\hat{q}_2) d\hat{q} d\hat{q}_2/(2\pi)^{2d+2}$$ (3.7)

re $\Lambda e^{-\ell} < q < \Lambda$ while $0 < q_2 < \Lambda$. The result (3.7) can be simplified in the rit of the renormalization group: we neglect both k and q_2 in compar- on with q for $\Lambda e^{-\ell} < q < \Lambda$. Since $P_{lmn}(\hat{q}) P_{luv}(\hat{q}) P_{\mu n}(\hat{q}) = 0$, some caution necessary here to keep the leading order non-vanishing term in the sulting integral. Performing the integration over $\underline{q}$ and neglecting $\underline{q}_2$ in parison with $\underline{q}$, where $q = (\hat{q},\Omega)$ and $\hat{q}_2 = (\hat{q}_2,\Omega_2)$, gives

$$\Delta\epsilon_1 = \frac{\lambda_0^2 D_0}{v_0^2} \int \frac{[q_m P_{n\mu\nu}(q) + q_n P_{m\mu\nu}(q)]}{q^9} \times$$

$$\times (q_2)_\mu (q_2)_n v_m^<(\hat{q}_2) v_\nu^<(k-\hat{q}_2) \frac{d^3 q d^3 q_2 d\mu_2}{(2\pi)^7}$$

Comparing expressions (3.8) and (2.9) gives the result

$$\Delta\epsilon_1 = \Delta\nu \int (q_2)_n (k-q_2)_m (\hat{q}_2) v_m^<(\hat{q}_2) v_\nu^<(k-\hat{q}_2) d\hat{q}_2/(2\pi)^4$$

in the limit $k \to 0$.
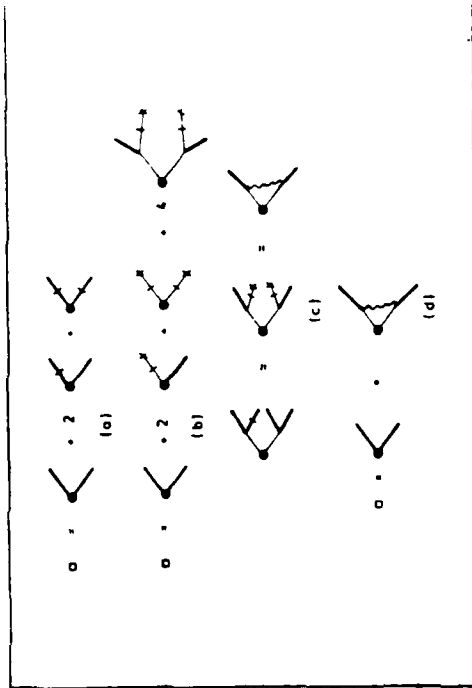

Fig. 2   A diagrammatic representation of the coarse-graining (renorma lization) of the dissipation rate ϵ, which is represented by t vertex, represented by the solid circle, is $v_0 q_\ell(k-q_\ell)$, while t dot vertex is $(1\lambda_0/2)P_{lmn}(k)$.
(a) Diagrammatic representation of (3.6).
(b) Irreducible diagram expansion of $\epsilon^<$.
(c) Second-order correction, included in (3.7).
(d) Diagrammatic representation of (3.7), which is asymptotically exact as $t \to 0$.

Here $C = (3\hat{A}_d/8(2\pi)^4/\epsilon^4 \approx 50$ since $\hat{A}_3 \approx 0.0118$ (see below) and $\epsilon \approx 0.2$. ramp function H appears in (3.13) because $\epsilon > 0$ in order for renormali-tion to be possible. The renormalized equation of motion for $v^<$ is thus

$$\frac{\partial \tilde{v}^<}{\partial t} + \tilde{v}^< \cdot \tilde{\nabla}\tilde{v}^< = -\frac{\nabla p}{\rho} + \tilde{f} + \nu_R \tilde{\nabla}\tilde{v}^< \tag{3.}$$

where ν_R given by (3.14), is related to $\tilde{\epsilon}$ by

$$\tilde{\epsilon} = \nu_R \left|\frac{\partial v^<_i}{\partial x_j} + \frac{\partial v^<_j}{\partial x_i}\right| \frac{\partial v^<_i}{\partial x_j} \tag{3.11}$$

The key assumptions in the derivation of (3.14) – (3.15) are that renormalized scales are locally homogeneous and isotropic and belong to inertial range characterized by the Kolmogorov $k^{-5/3}$ spectrum. Th implies that the eliminated scales are much smaller than the distance y the nearest wall, for only such scales can be isotropic. In the derivat of (3.14) – (3.15), we implicitly assume that $\Delta \ll y$ as well as v/Δ Thus, Δ must decrease as the distance to the nearest wall y decreases. It follows from (3.14) that $\nu_R \to \nu_0$ as $y \to 0$.

On the other hand, in the region far from the wall

$$\frac{3\hat{A}_d}{8(2\pi)^4} \tilde{\epsilon} \frac{\Delta^4}{\nu_0^3} \gg C$$

so that the solution to (3.14) is

$$\nu_R = \frac{1}{4}\left[\frac{3\hat{A}_d}{(2\pi)^4}\right]^{1/2}\Delta^2\left(\left|\frac{\partial v^<_i}{\partial x_j} + \frac{\partial v^<_j}{\partial x_i}\right|^2\right)^{1/2} \tag{3.}$$

which has the form of the classical Smagorinsky eddy viscosity (1.1). numerical coefficient in (3.16) is evaluated using $\hat{A}_3 \approx 0.23$ by (2.10). explicit expression for ν_R far from walls is

$$\nu_R = C_\nu \Delta^2 \left[\left|\frac{\partial v^<_i}{\partial x_j} + \frac{\partial v^<_j}{\partial x_i}\right|^2\right]^{1/2} \tag{3.}$$

with $C_\nu = 0.0053$.

In contrast to (3.17) the expression used by DEARDORFF [4] is give (3.17) with $C_\nu = 0.0070$. In stratified turbulence, DEARDORFF [5] ar

---

t follows from (3.9) and the corresponding result for the second integral n (3.5) (which is treated similarly) that, upon using the local homogene-ty assumption to transform back to physical space,

$$\epsilon(\tilde{x},t) = \nu(t)\left(\frac{\partial v^<_i}{\partial x_j} + \frac{\partial v^<_j}{\partial x_i}\right)\frac{\partial v^<_i}{\partial x_j} \tag{3.10}$$

here $\tilde{v}^<(\tilde{x},t)$ is defined as the inverse Fourier transform of $\hat{v}^<(k)$. The verse Fourier transform of $v^<$ is defined in the usual way as

$$\tilde{v}^<(\tilde{x},t) = \int_{-\infty}^{\infty} \hat{v}^<(k)e^{-ikx}e^{-i\omega t}dk\,d\omega \tag{3.11}$$

here the integrals may be taken with infinite range since high modes do ot contribute to the Fourier integral.

can be shown that $\epsilon(\tilde{x},t)$ given by expression (3.10) is independent of t n the limit of large t. Renormalizing only the subgrid scale motions, we entify $\epsilon^<$ derived above with $\tilde{\epsilon}$, which enters the definition of the random ce. Together with (2.15) and (3.10), this implies that

$$\tilde{\epsilon} = \frac{\nu_0}{2}\left[1 + \frac{3\hat{A}_d}{8}\frac{\tilde{\epsilon}}{\nu_0^4}\frac{\Delta^4}{4}(e^{4t}-1)\right]^{1/3}\left(\frac{\partial v^<_i}{\partial x_j} + \frac{\partial v^<_j}{\partial x_i}\right)^2$$

roducing the mesh size Δ as the smallest unrenormalized scale, i.e. $\tilde{\Delta} = \Delta^{-1} e$, and recalling that, in the Kolmogorov theory

$$\Delta = k_d = \pi(\tilde{\epsilon}/\nu_0^3)^{1/4} \tag{3.12}$$

ith $a \approx 0.2$ we obtain ($\Delta = 2\tilde{\Delta}$ is the half-width of the Gaussian filter, see IN & KIM [14]):

$$\tilde{\epsilon} = \frac{\nu_0}{2}\left[1 + H\left(\frac{3\hat{A}_d}{8(2\pi)^4}\frac{\tilde{\epsilon}}{\nu_0}\frac{\Delta^4}{3} - C\right)\right]^{1/3}\left(\frac{\partial v^<_i}{\partial x_j} + \frac{\partial v^<_j}{\partial x_i}\right)^2 \tag{3.13}$$

here $H(x) = x$ ($x > 0$), 0 ($x < 0$). It follows that the renormalized viscosity given by

$$\nu_R = \nu_0\left[1 + H\left(\frac{3\hat{A}_d}{8(2\pi)^4}\frac{\tilde{\epsilon}}{\nu_0}\frac{\Delta^4}{3} - C\right)\right]^{1/3} \tag{3.14}$$

that $C_v = 0.013$ worked better, but this is likely due to neglecting other effects of the stratification on the subgrid turbulence. MOIN & KIM [14] performed their simulations with $C_v = 0.003$. However, in order to prevent the turbulence in the wall region from decaying, MOIN & KIM redefined the average dissipation $\bar{\epsilon}$ as the turbulent dissipation.

$$\bar{\epsilon} = \frac{v_0}{2} \langle (S_{ij} - \langle S_{ij} \rangle)^2 \rangle \tag{3.18}$$

where

$$S_{ij} = \frac{\partial v_i}{\partial x_j} + \frac{\partial v_j}{\partial x_i}$$

and $\langle \rangle$ stands for the horizontal average over all scales. They also neglect the effect of the random forcing due to subgrid scale motions. MOIN & KIM [14] pointed out that their calculated turbulent intensities were insensitive to variations of the constant in (3.18) by ~40 %. Thus, we conclude that the agreement between calculated and "experimental" data are rather good.

Although the renormalized equation of motion derived in this section is basically the same as used far from the wall by DEARDORFF [4-7] and others, it differs significantly in the wall region where formula (3.16) is not valid. In the wall region the renormalized equations (3.13) - (3.15) do not lead to a turbulent-eddy viscosity proportional to A^2. Near the wall, the argument of $H( )$ in (3.14) is negative, so $v_R = v_0$.

Another important feature of finite systems is the role of the random force generated by elimination of small scales. This force is Gaussian with correlation function given by the diagrams presented in Fig. 1. The analytic expression for the correlation function corresponding to these diagrams follows from the second term on the right side of (2.6) and is:

$$\langle f_i(k) f_j(k') \rangle = D'(2\pi)^{d+1} k^2 \left[\delta_{ij} - \frac{k_i k_j}{k^2}\right] \delta(k+k') \delta(\omega-\omega') \tag{3.19}$$

with

$$D' = \frac{D_0^2 v_0^2}{2} \int \frac{d^d q}{(2\pi)^d} \frac{d\Omega}{2\pi} P_{\ell mn}(k) P_{\ell mu}(k) P_{mu}(q) P_{nu}(k-q) q^{-d}|k-q|^{-d} \times$$
$$\times |G^0(q)|^2 |G^0(k-q)|^2 \tag{3.20}$$

the integrals in (3.20) are readily evaluated giving

$$D' = \frac{A_d}{9} \frac{v_0^3}{k_d} \bar{\lambda}_0^4 \frac{e^{(d+7)\ell}-1}{d+7} \tag{}$$

A recursion relation for $D'(\ell)$ is derived using (2.15) and (2.16):

$$\frac{dD'}{d\ell} = \frac{A_d}{9} \frac{d}{d\ell}\left(\frac{\bar{\lambda}^4(\ell)v_0^3(\ell)}{k_d(\ell)}\right)$$

$$D'(0) = 0$$

so that

$$D' = \frac{A_d}{9} \frac{v_0^3 \bar{\lambda}_0^4}{k_d} \frac{(e^{9\ell}-1)}{1+(3A_d/4)\bar{\lambda}_0^2(e^{4\ell}-1)}$$
$$= \frac{2.09 \bar{\epsilon}}{k_d^5} \frac{H\{1.5 \times 10^{-8}(\bar{\epsilon}/v_0)^3 \Lambda^9 k_d^5 - 100\}}{1 + H(5.5 \times 10^{-5}(\bar{\epsilon}/v_0)^3 \Lambda^4 - 100)} \tag{}$$

It should be emphasized that RNG procedures dealing with infinite systems neglect the induced random force (3.19) in the limit $k \to 0$, because the correlation function is proportional to k^2, which is small in comparison with the correlation $O(k^{-3})$ of the bare force. However, in finite systems where k is bounded from below, the role of the induced force should be reassessed. Far from the wall where $\{A_d \bar{\lambda}_0^2 e^{4\ell} = \frac{3}{4} A_d \frac{\bar{\epsilon}}{v_0} \Lambda^3 e^{4\ell} >> 1$ we obtain from (2.25):

$$D' = \frac{v_0^3 \bar{\lambda}_0^2}{k_d} e^{5\ell} = \frac{v_0^3 \bar{\lambda}_0^2}{k_d} \left(\frac{k_d}{k_c}\right)^5 \tag{}$$

where $k_c = k_d e^{-\ell}$ is the mode cutoff for the RNG. Thus the condition for induced force to be small when compared to the bare force is

$$\frac{v_0^3 \bar{\lambda}_0^2}{k_d} \left(\frac{k_d}{k_c}\right)^5 k^2 < \frac{D_0}{k^3} \tag{}$$

which holds provided that

$$\left(\frac{k}{k_c}\right)^5 < 1 \quad (k_c << k_d, \quad k \leq k_c) .$$

Thus, far from walls, the RNG induced force is negligible.

However, in the buffer region, defined by the condition

$$1 \cdot \frac{3}{4} A_d \bar{1}_0^2 e^{4\tau} = O(\tau) = O(100)$$

he ratio of the RNG induced force to the bare force is

$$\left(\frac{k}{k_d}\right)^5 \frac{v_0^3 k_d^3}{D_0} \frac{\bar{1}_0}{1 \cdot \frac{3}{4} A_d \bar{1}_0^2} \frac{A_d (e^{9\tau}-1)}{(e^{4\tau}-1)} \cdot 1 \tag{3.25}$$

...ided that

$$\frac{k}{k_d} \cdot 0.1 \tag{3.26}$$

ting that $\bar{1}_0^2 = 2D_0/v_0^3 k_d^3 = O(1)$.

hus in the narrow region of scales satisfying

$$0.1 \, k_d < k < k_c \tag{3.27}$$

th

$$A_d e^{4\tau} = A_d \left(\frac{k_d}{k_c}\right)^4 \sim 1 \tag{3.28}$$

he induced force is larger than the bare stirring forces and cannot be eglected.

nequalities (3.28) - (3.29) define the wave vector range in the buffer ayer where the induced RNG force cannot be omitted. Without the action of his random force, the turbulence in the buffer layer is likely to decay e to the enhanced (renormalized) viscosity.

DISCUSSION AND CONCLUSIONS

this work we used renormalization-group ideas in order to systemat ally eliminate small scales and construct a subgrid model. The need for systematic procedure is demonstrated by the formula (3.14) for the ity v_R which, in the wall region, differs quite substantially from Smagorinski expression. It has become clear from the recent studies of large-eddy simulation (MOIN & KIM [14]) that the extrapolation of the rinski formula up to the wall does not lead to satisfactory results, additional turbulence modelling is needed to achieve agreement experimental data. The expression for the turbulent viscosity

derived here agrees well with formulas used by DEARDORFF [4] and MOIN & [14] far from the wall. We expect that this formulation will provide a g description of the entire flow in the channel.

Another outcome of the present theory is the appearance of the ran force as a result of small-scale elimination. This result deserves further comment. BARDINA, FERZIGER & REYNOLDS [1] compared different grid models for homogeneous turbulence. They showed that simply using the Smagorinski results in quite low correlation coefficients the subgrid scale stresses with those produced in full numerical solutio of the Navier-Stokes equations, especially for homogeneous shear turb lence.

BARDINA et al. [1] also introduced a so-called scale-similarity model the subgrid scale, which represented the Reynolds stress R_{ij} in Navier-Stokes equation in terms of filtered scales $u_i' = u_i - \bar{u}_i$ where u_i, $\bar{u}_i$ are the exact and large-eddy velocity, respectively. That is, the r grid stresses on scales from 0 to Δ are approximated as the filter stre that involved scales between, for example, Δ and 2Δ. That is

$$R_{ij} \sim u_i u_j - \bar{\bar{u}}_i \bar{\bar{u}}_j \tag{3}$$

where $\bar{\bar{u}}_i$ is the velocity field filtered over 2Δ. BARDINA et al. [1] sho that this model gives a correct representation of turbulence intensiti However, they also showed that this scale-similarity model is not dissi tive, so it is unable to describe the decay of turbulence. They showed the a linear combination of these two models is good for a description of h turbulent intensities and dissipative processes, at least in homogene turbulence. It is easy to see from (4.1) that $\bar{R}_{ij} = 0$, which implies the $\bar{R}_{ij} \cdot O(k^2)$ when $k \cdot 0$. Thus R_{ij}, as proposed by BARDINA et al. [1], h the properties of the random force that we have derived here. It i essential result of the present theory that one must take into acco both the eddy viscosity and the random force since they appear simultan ously as a result of the elimination of small scales.

It can be shown (YAKHOT & ORSZAG, to be published) that, when additio physical processes such as rotation, etc. are acting, the equations the large-eddy simulations based on the present renormalization-gr method include many new terms which are usually not taken into account large-eddy simulations.

REFERENCES

[1] J. BARDINA, J. FERZIGER, W.C. REYNOLDS: to be published (1983).

[2] M.E. RPACHET, D.I. MEIRON, S.A. ORSZAG, B.G. NICKEL, R.H. MORF, U. FRISCH: J. Fluid Mech. 130, 411 (1983).

[3] G. COMTE-BELLOT: Écoulement turbulent entre deux parois paralleles. Publications Scientifiques et Techniques du Ministere de l'Air, no. 419 (1965).

[4] J.W. DEARDORFF: J. Fluid Mech. 41, 453 (1970).

[5] J.W. DEARDORFF: J. Comp. Phys. 7, 120 (1971).

[6] J.W. DEARDORFF: J. Atmos. Sci. 29, 91 (1972).

[7] J.W. DEARDORFF: J. Fluids Eng. 429 (1973).

[8] D. FORSTER, D.R. NELSON, M.J. STEPHEN: Phys. Rev. A16, 732 (1977).

[9] J.-D. FOURNIER, U. FRISCH: Phys. Rev. A28, 1000 (1983).

[10] S.J. KLINE, W.C. REYNOLDS, F.A. SCHRAUB, P.W. RUNSTADLER: J. Fluid Mech. 30, 741 (1967).

[11] R.H. KRAICHNAN: J. Math. Phys. 2, 124 (1961).

[12] D.K. LILLY: in Proc. IBM Sci. Comp. Symp. on Environmental Sciences, White Plains, New York, p.195 (1967).

[13] P.C. MARTIN, C. DeDOMINICIS: Phys. Rev. A19, 419 (1979).

[14] F. MOIN, J. KIM: J. Fluid Mech. 118, 341 (1982).

[15] E.A. NOVIKOV: JETP 47, 5 (1964).

[16] S.A. ORSZAG, A.T. PATERA: Phys. Rev. Letters 47, 832 (1981).

[17] E.R. VAN DRIEST: J. Aero. Sci. 23, 1007 (1956).

[18] H.W. WYLD: Ann. Phys. (N.Y.) 14, 143 (1961).

[19] V. YAKHOT: Phys. Rev. A23, 1486 (1981).

METEOROLOGICAL DYNAMICS

THREE DIMENSIONAL CUMULUS CLOUD CONVECTION

U. SCHUMANN

1. INTRODUCTION

1.1 Objective

A cloud can be defined as a visible ensemble or aggregate of so-ca hydrometers, i.e., minute particles consisting of liquid or frozen w in a wide variety of forms. The processes involved in the formation clouds range from the very small-scale processes responsible for nucleation and growth of cloud particles (cloud microphysics) up to very large-scale dynamical processes that are associated with synct weather systems. A large portion of the study of clouds has been focuse their microphysical processes, evidenced by the voluminous material cloud microphysics, with less attention paid to the dynamics of cloud f mation, COTTON, LILLY [1,2]. Much has been learned in recent years at the structure of strong convection, with the help of observational to particularly doppler-radar, BROWNING, SCHROTH [3,4]. With the advent powerful scientific computers such as the CRAY-1, substantial advance numerical modelling of cumulus convection has been achieved up to now, even more can be expected in the near future, SCHLESINGER [5].

The objective of this paper is to show the importance and potential of dies of nonlinear fluid dynamics aspects, the need for three-dimensir simulation models together with suitable field observations, and the j sent state of research in the field.

1.2 Cloud genera

This paper focuses on clouds of convective origin. Meteorologists comm ly reserve the word convection for vertical flows, while the term adv tion is introduced to indicate horizontal transport.

Three conditions often viewed necessary for cloud formation from a pat of moist air are 1) a sufficient amount of water vapour, 2) a proper d tribution of condensation and ice nuclei, and 3) a process that cools

Lectures on Spectral Methods for Turbulence Computations.

S. A. ORSZAG (*)

Massachusetts Institute of Technology - Cambridge, MA 02139

1. – Introduction to spectral methods.

Spectral methods are based on representing the solution to a problem as a truncated series of smooth functions of the independent variables. Whereas finite-element methods are based on expansions in local basis functions, spectral methods are based on expansions in global functions. Spectral methods are the extension of the standard technique of separation of variables to the solution of arbitrarily complicated problems.

Let us begin by illustrating spectral methods for the simple one-dimensional heat equation. Consider the mixed initial-boundary-value problem

$$(1.1) \qquad \frac{\partial u(x, t)}{\partial t} = K \frac{\partial^2 u(x, t)}{\partial x^2} \qquad (0 < x < \pi, t > 0),$$

$$(1.2) \qquad u(0, t) = u(\pi, t) = 0 \qquad (t > 0),$$

$$(1.3) \qquad u(x, 0) = f(x) \qquad (0 < x < \pi).$$

The solution to this problem is

$$(1.4) \qquad u(x, t) = \sum_{n=1}^{\infty} a_n(t) \sin nx,$$

$$(1.5) \qquad a_n(t) = f_n \exp[-Kn^2 t],$$

where

$$(1.6) \qquad f_n = \frac{2}{\pi} \int_0^{\pi} f(x) \sin nx \, dx$$

are the coefficients of the Fourier sign series expansion of $f(x)$.

(*) Present address: Princeton University, Princeton, NJ 08540.

A spectral approximation to (1.1)-(1.3) is gotten by simply truncating (1.4) to

$$(1.7) \qquad u_N(x, t) = \sum_{n=1}^{N} a_n(t) \sin nx$$

and replacing (1.5) by the evolution equation

$$(1.8) \qquad \frac{da_n}{dt} = -Kn^2 a_n \qquad (n = 1, \ldots, N)$$

with the initial conditions $a_n(0) = f_n$ $(n = 1, \ldots, N)$.

The spectral approximation (1.7), (1.8) to (1.1)-(1.3) is an exceedingly good approximation for any time t greater than zero as $N \to \infty$. In fact, the error $u(x, t) - u_N(x, t)$ satisfies

$$(1.9) \qquad u(x, t) - u_N(x, t) = \sum_{n=N+1}^{\infty} f_n \exp[-Kn^2 t] \sin nx = O(\exp[-KN^2 t])$$
$$(N \to \infty)$$

for any $t > 0$. In contrast to (1.9), finite-difference approximations to the heat equation using N grid points in x lead to errors that decay only algebraically with N as $N \to \infty$. Furthermore, this spectral method for the solution of the heat equation is efficiently implementable by the fast Fourier transform (FFT) in $O(N \log N)$ operations.

There are several significant difficulties in extending the simple spectral method employed for (1.1)-(1.3) to more general problems. Among these difficulties are those caused by imposition of nontrivial boundary conditions, nonlinear and nonconstant coefficient terms, and complex geometries. These difficulties and their solutions will be discussed below (see also [1, 2]).

The Fourier series (1.4) converges fast if $u(x, t)$ is infinitely differentiable and $u(x, t)$ satisfies the boundary conditions

$$(1.10) \qquad \frac{\partial^{2n} u(x, t)}{\partial x^{2n}} = 0 \qquad (x = 0, \pi)$$

for all nonnegative integers n. Under these conditions, the error after N terms

$$\epsilon_N(x, t) = u(x, t) - \sum_{n=1}^{N} a_n(t) \sin nx$$

goes to zero uniformly in x faster than any power of $1/N$ as $N \to \infty$. On the other hand, if $u(x, t)$ is not infinitely differentiable or if any of the conditions (1.10) is violated, then $\epsilon_N(x, t) = O(1/N^p)$ as $N \to \infty$ for some finite p. For

example,

$$(1.11) \qquad 1 = \sum_{n=0}^{\infty} (-1)^n \frac{\sin (2n+1)x}{2n+1} \qquad (0 < x < \pi),$$

but the error incurred by truncating after N terms is of order $1/N$ for any fixed $x, 0 < x < \pi$. Furthermore, the convergence of (1.11) is not uniform in x; (1.11) exhibits Gibbs' phenomenon, namely

$$\varepsilon_N(\xi/N) = O(1) \qquad (N \to \infty, \ \xi \ \text{fixed}).$$

For any fixed N, there are points x at which the error after N terms of (1.11) is not small. The poor convergence of (1.11) is due to the violation of (1.10) for $n = 0$.

More generally, most eigenfunction expansions of a function $f(x)$ converge faster than algebraically (*i.e.* the error incurred by truncating after N terms goes to zero faster than any finite power of $1/N$ as $N \to \infty$) only if $f(x)$ is infinitely differentiable *and* $f(x)$ satisfies an infinite number of special boundary conditions. For example, the Fourier-Bessel expansion

$$f(x) = \sum_{n=0}^{\infty} a_n J_0(\lambda_n x) \qquad (0 < x < 1),$$

where λ_n is the n-th smallest root of $J_0(\lambda) = 0$, converges faster than algebraically only if f is infinitely differentiable and

$$(1.12) \qquad \left[\frac{1}{x} \frac{d}{dx} x \frac{d}{dx}\right]^k f(x) = 0 \qquad \text{at } x = 1$$

for $k = 0, 1, 2, \ldots$.

When a spectral expansion converges only algebraically fast, spectral methods based on these eigenfunction expansions cannot offer significant advantages over more conventional (finite-difference, finite-element) methods. Eigenfunction expansions of this kind should not normally be used *unless* the boundary conditions of the problem imply all the extra boundary constraints like (1.10) or (1.12). For example, if periodic boundary conditions are compatible with the differential equation to be solved, complex Fourier series are suitable to develop efficient spectral approximations.

In the development of spectral methods for general problems, it is important that the rate of convergence of the eigenfunction expansion being used does not depend on special properties of the eigenfunctions, like boundary conditions, but rather depend only on the smoothness of the function being expanded. Of course, if the solution to the problem being solved is not smooth, one should not expect errors that decrease faster than algebraically with $1/N$ when global

eigenfunction expansions are used. Faster than algebraic rates of convergence may be achieved for these problems by either patching the solution at discontinuities or pre- and post-processing of the solution (see [2]).

There is an easy way to ensure that the rate of convergence of a spectral expansion of a function $f(x)$ depends only on the smoothness of $f(x)$, not on its boundary properties. The idea is to expand in terms of suitable classes of orthogonal polynomials, including Chebyshev and Legendre polynomials for all those problems in which constraints like (1.10) and (1.12) are unrealistic. These polynomial expansions avoid all difficulties associated with the Gibbs phenomenon provided the solution $f(x)$ is smooth.

From the mathematical point of view, the classical orthogonal polynomials are eigenfunctions of singular Sturm-Liouville problems. It is not hard to show [1] that expansions using eigenfunctions of such singular Sturm-Liouville problems converge at a rate that depends only on the smoothness of $f(x)$, in contrast to eigenfunction expansions based on nonsingular Sturm-Liouville problems that lead to additional boundary constraints like (1.10) on $f(x)$.

These results for orthogonal polynomial expansions are easily demonstrated in the case of Chebyshev polynomial expansions. The n-th–degree Chebyshev polynomial $T_n(x)$ is defined by

(1.13)
$$T_n(\cos\theta) = \cos n\theta .$$

Therefore, if

(1.14)
$$f(x) = \sum_{n=0}^{\infty} a_n T_n(x) ,$$

then

(1.15)
$$g(\theta) = f(\cos\theta) = \sum_{n=0}^{\infty} a_n \cos n\theta .$$

Thus the Chebyshev polynomial expansion coefficients a_n of $f(x)$ are just the Fourier cosine expansion coefficients of the even, periodic function $g(\theta)$. A simple integration-by-parts argument then shows that

$$n^p a_n \to 0 \qquad\qquad (n \to \infty) ,$$

provided $g(\theta)$ (or, equivalently, $f(x)$) has p continuous derivatives. Since

$$\left| f(x) - \sum_{n=0}^{N} a_n T_n(x) \right| < \sum_{n=N+1}^{\infty} |a_n| \qquad\qquad (|x|<1) ,$$

it follows that the rate of convergence of (1.14) is faster than algebraic if f is smooth.

In summary, spectral expansions should be made using series of orthogonal polynomials unless the boundary conditions of the problem are fully compatible with some other class of eigenfunctions. In practice, Chebyshev and Legendre polynomial expansions are recommended for most applications, supplemented by Fourier series and surface harmonic series when boundary conditions permit.

Another difficulty with general kinds of spectral methods is their application to problems with nonlinear and nonconstant coefficient terms. Before explaining the solution to this problem, let us illustrate the difficulty.

Suppose we wish to solve the partial differential equation

$$(1.16) \qquad \frac{\partial u}{\partial t} = \mathcal{N}(u, u) + \mathcal{L}u,$$

where $u = u(x, t)$ and $\mathcal{N}$ is a bilinear (nonlinear) operator that involves only spatial derivatives and $\mathcal{L}$ is a linear operator that involves only spatial derivatives. The operators $\mathcal{N}$ and $\mathcal{L}$ may depend on both x and t. A spectral method for the solution of (1.16) is obtained by seeking the solution as a finite spectral expansion:

$$(1.17) \qquad u(x, t) = \sum_{n=1}^{N} a_n(t)\psi_n(x),$$

where we assume for now that $\psi_n(x)$ $(1 < n < \infty)$ are a complete set of orthogonal functions. If we introduce the re-expansion coefficients c_{nmp} and d_{nm} so that

$$\mathcal{N}(\psi_m, \psi_p) = \sum_{n=1}^{\infty} c_{nmp}(t)\psi_n,$$

$$\mathcal{L}(\psi_m) = \sum_{n=1}^{\infty} d_{nm}(t)\psi_n$$

and equate coefficients of $\psi_n(x)$ $(n = 1, ..., N)$ in (1.16), we obtain

$$(1.18) \qquad \frac{da_n}{dt} = \sum_{m=1}^{N} \sum_{p=1}^{N} c_{nmp}(t)a_m(t)a_p(t) + \sum_{m=1}^{N} d_{nm}(t)a_m(t) \qquad (n = 1, ..., N).$$

Equations (1.18) are the spectral evolution equations for the solution of (1.16). They have one very serious drawback. In general c_{nmp} and d_{nm} are nonzero for typical n, m, p, so that evaluation of da/dt from (1.18) for all $n = 1, ..., N$ requires $O(N^3)$ arithmetic operations for the bilinear term and $O(N^2)$ operations for the linear term. Thus solution of (1.18) requires order N^3 operations per time step. Since operational spectral calculations now involve $N \gtrsim 10^6$, the computational cost of the direct solution of (1.18) is prohibitive (even if only linear terms are present).

The problem here is one of computational complexity. Finite-difference methods for the solution of (1.16) on N grid points may require only order N operations per time step. If the spectral method really requires order N^3 operations per time step, it cannot compete when N is large.

Another example illustrating the computational complexity of spectral methods is given by the nonlinear diffusion equation

$$(1.19) \qquad \frac{\partial u(x, t)}{\partial t} = \exp [u] \frac{\partial^2 u}{\partial x^2} (x, t) .$$

If we seek the solution as

$$(1.20) \qquad u(x, t) = \sum_{n=1}^{N} a_n(t) \psi_n(x)$$

in terms of the orthonormal functions $\psi_n(x)$, then

$$(1.21) \qquad \frac{\mathrm{d}a_n}{\mathrm{d}t} = \int \psi_n(x) \exp \Big[\sum_{m=1}^{N} a_m(t) \psi_m(x) \Big] \sum_{p=1}^{N} a_p \psi_p''(x) \, \mathrm{d}x$$

for $n = 1, ..., N$. These evolution equations for $\{a_n(t)\}$ have an exponential degree of computational complexity as they are expressed as an integral functional of $\{a_n(t)\}$.

The solution to the problem of computational complexity is to use the author's transform methods. Let us illustrate the technique for a pseudo-spectral (or collocation) approximation to (1.19). First, we introduce N suitable collocation points $x_1, x_2, ..., x_N$ lying within the computational domain. Then the approximate solution (1.20) is forced to satisfy the partial differential equation (1.19) (or its boundary conditions) exactly at these discrete points at every time t. More specifically, the following three steps are done at each time step t:

i) Determine N coefficients $a_n(t)$ $(n - 1, ..., N)$ so that

$$(1.22) \qquad u(x_j, t) = \sum_{n=1}^{N} a_n(t) \psi_n(x_j) \qquad\qquad (j = 1, ..., N) .$$

ii) Evaluate $u_{xx}(x_j, t)$ by

$$(1.23) \qquad u_{xx}(x_j, t) = \sum_{n=1}^{N} a_n(t) \psi_n''(x_j) \qquad\qquad (j = 1, ..., N) .$$

iii) Finally, evaluate $\partial u(x_j, t)/\partial t$ by

$$(1.24) \qquad \frac{\partial u(x_j, t)}{\partial t} = \exp [u(x_j, t)] u_{xx}(x_j, t) \qquad\qquad (j = 1, ..., N)$$

and march forward to the next time step.

The idea of the pseudospectral transform method can be restated as follows: Transform freely between physical (x,) and spectral (a_n) representations, evaluating each term in whatever representation that term is most accurately, and simply, evaluated. Thus, in (1.24), we evaluate exp [u] in the physical representation while we compute u_{xx} in the spectral representation by (1.22) because it is most accurately done there.

It should be apparent to the reader that pseudospectral transform methods can be applied to any problem that can be treated by finite-difference methods regardless of the technical complexity of nonlinear and nonconstant coefficient terms.

For the expressions of interest, computation of derivatives of a N-term spectral expansion requires order N arithmetical operations. For the Fourier series (1.7), this fact is obvious:

$$\frac{d}{dx} \sum_{n=1}^{N} a_n \sin nx = \sum_{n=1}^{N} na_n \cos nx \,,$$

$$\frac{d^2}{dx^2} \sum_{n=1}^{N} a_n \sin nx = - \sum_{n=1}^{N} n^2 a_n \sin nx \,.$$

For the Chebyshev polynomial expansion (1.14), the computational complexity of differentiation is a little less apparent. Since $T_n(\cos \theta) = \cos n\theta$,

$$\frac{T'_{n+1}(x)}{n+1} - \frac{T'_{n-1}(x)}{n-1} = \frac{2}{c_n} T_n(x) \qquad (n>0) \,,$$

where $c_0 = 2$, $c_n = 1$ $(n>1)$ and $T'_0 = T'_{-1} = 0$. Therefore, if

$$\frac{d}{dx} \sum_{n=0}^{N} a_n T_n(x) = \sum_{n=0}^{N} b_n T_n(x) \,,$$

then

$$2 \sum_{n=1}^{N} a_n T'_n(x) = \sum_{n=0}^{N} c_n b_n \left[\frac{T'_{n+1}}{n+1} - \frac{T'_{n-1}}{n-1} \right] = \sum_{n=1}^{N+1} [c_{n-1} b_{n-1} - b_{n+1}] T'_n(x)/n \,.$$

Equating coefficients of $T'_n(x)$ for $n = 1, ..., N+1$ gives the recurrence relation

$$(1.25) \qquad \begin{cases} c_{n-1} b_{n-1} - b_{n+1} = 2na_n & (1 < n < N) \,, \\ b_n = 0 & (n > N) \,. \end{cases}$$

The solution of (1.25) for b_n given a_n requires only order N arithmetic operations. Similar recurrence relations can be obtained for differentiation of spectral series based on other sets of orthogonal polynomials and functions.

In the case of Fourier series, the transform (1.7) and its inverse can be computed in $O(N \log_2 N)$ operations if $N = 2^p$ using the fast Fourier transform. However, most of the computational efficiency of transform methods comes not from the FFT but from the separability of multidimensional transforms. Thus a three-dimensional discrete Fourier transform can be expressed as three one-dimensional Fourier transforms

$$(1.26) \quad \sum_{j=0}^{J-1} \sum_{k=0}^{K-1} \sum_{l=0}^{L-1} a(j, k, l) \exp\left[2\pi i \left(\frac{jm}{J} + \frac{kn}{K} + \frac{lp}{P}\right)\right] =$$

$$= \sum_{j=0}^{J-1} \exp\left[2\pi i jm/J\right] \sum_{k=0}^{K-1} \exp\left[2\pi i kn/K\right] \sum_{l=0}^{L-1} a(j, k, l) \exp\left[2\pi i lp/L\right].$$

The left-hand side of (1.26) requires roughly $(JKL)^2$ operations to evaluate at all the points $0 < m < J$, $0 < n < K$, $0 < p < L$. On the other hand, even without the FFT, the right-hand side of (1.26) requires only about $(JKL)\cdot(J + K + L)$ operations to evaluate at all the points. When the FFT is applied to the one-dimensional transforms on the right-hand side of (1.26), the number of operations necessary to evaluate (1.26) is reduced further to $(JKL)\cdot(\log_2 J + \log_2 K + \log_2 L)$ if J, K, L are powers of 2.

Spectral approximations to general boundary-value problems lead to full $N \times N$ matrix equations for the N expansion coefficients a_n. It would seem that solution of these equations requires $O(N^3)$ arithmetic operations, while storage of the matrix requires $O(N^2)$ memory locations. Since typical problems now involve $N \sim 10^6$, the direct solution (or even the direct formulation) of such problems would seem unworkable now.

Consider the solution of a general linear differential equation $Lu = f$. Let a N-term spectral approximation to this problem be given by

$$(1.27) \qquad\qquad L_{sp} u_N = f_N,$$

where f_N is a suitable N-term approximation to f. As mentioned several times earlier, the matrix representation of (1.27) is generally a full $N \times N$ matrix, so that direct solution of (1.27) by Gauss elimination methods would require order N^2 storage (for the matrix representation of L_{sp}) and order N^3 arithmetic operations.

Here we shall describe a method that permits the solution of (1.27) using order N storage locations with the number of arithmetic operations of order the larger of $N \log N$ and the number of operations required to solve $Lu = f$ by a *first-order* finite-difference method. The important conclusion is that *spectral methods for general problems in general geometries can be implemented efficiently with operation costs and storage not much larger than that of the simplest finite-difference approximation to the problem with the same number of degrees of freedom*. Since spectral methods require many fewer degrees of freedom to

achieve given accuracy (or, nearly equivalently, spectral methods achieve much higher accuracy for a given number of degrees of freedom) than required by finite-order finite-difference approximations, important computational efficiencies result from the new method.

The idea of the iteration method is as follows: Suppose we are able to construct an approximation L_{ap} to the spectral operator L_{sp} that has the following properties:

  i) L_{ap} has a sparse matrix representation so that it can be represented using only $O(N)$ storage locations.

  ii) L_{ap} is efficiently invertible in the sense that the equation

$$(1.28) \qquad\qquad L_{ap} u_N = f_N$$

is solvable as efficiently as a first-order finite-difference approximation to the problem.

  iii) L_{ap} approximates L_{sp} in the sense that

$$(1.29) \qquad\qquad 0 < m < \| L_{ap}^{-1} L_{sp} \| < M < \infty$$

for suitable constants m, M as $N \to \infty$. Roughly speaking, (1.29) requires that the eigenvalues of $L_{ap}^{-1} L_{sp}$ be bounded from above and below as $N \to \infty$.

We propose to construct L_{ap} from L_{sp} by changing the discretization operator either in addition to or in place of approximating the differential operator. Thus we construct L_{ap} by a suitable *low-order finite-difference approximation to L*.

A simple example is given by the second-order differential equation

$$(1.30) \qquad Lu = f(x) u''(x) + g(x) u'(x) + h(x) u(x) = r(x) \qquad (0 < x < 2\pi)$$

with periodic boundary conditions $u(x + 2\pi) = u(x)$ and $f(x) > 0$. A spectral approximation is approximately sought as the finite Fourier series

$$(1.31) \qquad\qquad u(x) = \sum_{|k| < K} a_k \exp[ikx].$$

If the Fourier coefficients of $f(x)$, $g(x)$, $h(x)$, $r(x)$ are denoted f_k, g_k, h_k, r_k, respectively, then the spectral (Galerkin) equations for a_k are

$$(1.32) \qquad L_{sp} u = \sum_{\substack{|p| < K \\ |k-p| < K}} [-p^2 f_{k-p} + ipg_{k-p} + h_{k-p}] a_p = r_k.$$

Clearly, these equations have, in general, a full matrix representation that requires $O(K^2)$ storage locations and $O(K^3)$ operations to invert.

A suitable approximate operator L_{ap} is constructed using the collocation points $x_j = 2\pi j/N$ ($j = 0, 1, ..., N-1$), where $N = 2K$. In the physical space representation, we use the finite-difference approximation

$$(1.33) \qquad L_{ap} u'_{x_j} = f(x_j) \frac{u_{j+1} - 2u_j + u_{j-1}}{(\Delta x)^2} + g(x_j) \frac{u_{j+1} - u_{j-1}}{2\Delta x} + h(x_j)u_j.$$

where $u_j = u(x_j)$ and $\Delta x = 2\pi/N$. Obviously, L_{ap} is sparse and efficiently invertible. To verify (1.29) we use the following elementary argument (that may be made more rigorous but no more correct by more involved WKB-like arguments). If λ is an eigenvalue of $L_{ap}^{-1} L_{sp}$, then there exists a function $u(x)$ such that

$$(1.34) \qquad L_{sp} u = \lambda L_{ap} u.$$

If $u(x)$ is a smooth function of x (in the limit $N \to \infty$), then both $L_{ap} u$ and $L_{sp} u$ should be good approximations to $Lu(x)$, so (1.34) implies $\lambda \sim 1$. On the other hand, if $u(x)$ is a highly oscillatory function of x (in the limit $N \to \infty$), then

$$(1.35) \qquad u'' \gg u' \gg u \qquad (N \to \infty).$$

Therefore,

$$(1.36) \qquad L_{ap} u \sim f(x_j) \frac{u_{j+1} - 2u_j + u_{j-1}}{(\Delta x)^2}$$

and, if transform (pseudospectral) methods are used to evaluate $L_{sp} u$,

$$(1.37) \qquad L_{sp} u \sim f(x_j) \sum_{|k| < K} (-k^2) a_k \exp[ikx_j].$$

so (6.18) gives

$$(1.38) \qquad f(x_j) \sum_{|k| < K} (-k^2) a_k \exp[ikx_j] \sim \lambda f(x_j) \frac{u_{j+1} - 2u_j + u_{j-1}}{(\Delta x)^2}.$$

The eigenfunctions of (1.38) are

$$u_j = \exp[iqx_j] \qquad (|q| < K)$$

and the associated eigenvalue is

$$\lambda = \frac{(q\Delta x)^2}{4\sin^2 \frac{1}{2} q\Delta x}.$$

Since $q^2 < K$ with $K = \frac{1}{2}N = \pi/\Delta x$, we obtain

$$1 - \lambda = \frac{\pi^2}{4}.$$

Thus (1.29) holds with $m = 1$ and $M = \pi^2/4 \approx 2.5$.

There are several extensions of the above method for constructing L_{ap} that are important in practice. First, in the case of Chebyshev spectral methods, it is appropriate to construct L_{ap} using finite-difference approximations based on the collocation points $x_j = \cos \pi j/N$. In this case, the operator bounds (1.29) continue to hold with $M = 2.5$, $m = 1$ for a wide variety of operators L. Second, higher-order equations are best treated by writing them as a system of lower-order equations. Thus direct construction of L_{ap} for $L = \nabla^4$ gives

$$1 \leqslant \| L_{\text{ap}}^{-1} L_{\text{sp}} \| \leqslant 6 \approx \left(\frac{\pi^2}{4} \right)^2 .$$

However, if we introduce $v = \nabla^2 u$ and define the second-order operator K by

$$K \begin{pmatrix} u \\ v \end{pmatrix} = \begin{cases} \nabla^2 u - v , \\ \nabla^2 v , \end{cases}$$

then direct construction of K_{ap} as a finite-difference operator gives

$$1 < \| K_{\text{ap}}^{-1} K_{\text{sp}} \| \leqslant 2.5 .$$

Third, odd-order operators, initial-value problems and problems of mixed type are best treated by constructing L_{ap} on a grid that is roughly 50% finer than that used in construction of L_{sp} by collocation. In this case the spectral bounds (1.29) with $M \leqslant 2.5$ continue to hold for most problems. For example, the operator $\partial/\partial x$ with periodic boundary conditions has spectrum ik, while its centered finite-difference approximation has spectrum $i \sin (k\Delta x)/\Delta x$, so

$$\| L_{\text{ap}}^{-1} L_{\text{sp}} \| = O(k \Delta x/\sin k \Delta x) ,$$

which is unbounded for $|k \Delta x| < \pi$, but bounded by $4\pi/3\sqrt{3} \approx 2.4$ if $|k \Delta x| < 2\pi/3$.

2. – Applications.

2`1. Introduction. – Over the last few years, there has been progress in understanding fundamental nonlinear processes in shear flows. In this section, I shall survey some results that have emerged from numerical studies of tran-

sition and turbulence. I shall review for you three different aspects of these problems. First, I shall summarize results on the basic instabilities that seem to be responsible for the onset of chaos in these flows. These instabilities appear to be universal in character and may explain many of the unifying features of transition. Second, I shall give some examples of progress in the numerical simulation of high-Reynolds-number flows. Finally, I will give a synopsis of new ideas for subgrid scale closures of huge-Reynolds-number turbulence.

Full details of the ideas discussed here are given in the references.

2`2. *A transitional instability.* – The processes by which laminar flows undergo transition to turbulence remain basically unsolved. However, recent numerical studies have provided some insights into transition, including:

2`2.1. Nonclassical character of transitional instabilities. The primary linear (exponential) instability of classical plane parallel shear flows with noninflectional velocity profiles, as described by the Orr-Sommerfeld (or related) equations, is much too weak to describe transition. For example, linear instability of plane Poiseuille flow $(U(z) = 1 - z^2, |z| < 1)$ occurs for Reynolds numbers $R_c > 5778$, while Squire's theorem implies that the critical disturbance is two-dimensional. The fact that this instability is induced by a subtle interplay of viscosity and shear implies that its growth rates are quite small on convective time scales. For example, the most rapidly growing exponential mode of the Orr-Sommerfeld equation is obtained at $R_{opt} = 48000$; its growth rate is only 0.0076; it is so feeble that perturbations grow by a factor 10 in a time of about 300, in which time a point on the centerline moves about 150 channel widths. In contrast, transition is observed to occur explosively over a few channel widths at Reynolds numbers as low as roughly 1000. A transitional instability that affects noninflectional plane parallel shear flows must have a characteristic convective time scale.

2`2.2. Three dimensionality of transition. Two-dimensional fluids do not appear to exhibit the kind of strong chaos that is characteristic of turbulent shear flows. In thermal convection, CURRY *et al.* [3] show that two-dimensional flows do not appear to act in a strongly chaotic way, but three-dimensional flows may be strongly chaotic at large enough Reynolds number. Even for inflectional free shear flows, in which there are strong inviscid two-dimensional instabilities, BRACHET and ORSZAG [4] show that the flows that develop from two-dimensional finite-amplitude disturbances are not strongly chaotic, in contrast to the flows that develop three-dimensionally.

2`2.3. Instability of two-dimensional nonlinear travelling waves. Perhaps the simplest instability that has the character of a transitional instability is the linear three-dimensional instability of two-dimensional finite-amplitude flows. ORSZAG and KELLS [5] and ORSZAG and PATERA [6]
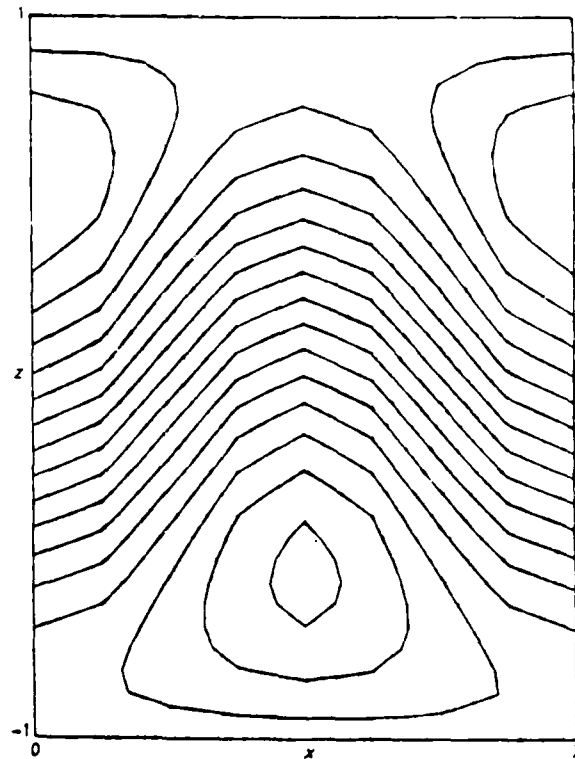
Fig. 1. — Streamlines of the steady (stable) finite-amplitude two-dimensional travelling wave for plane Poiseuille flow at $R = 4000$, plotted in the rest frame of the wave (from [6]).

show how such an instability fits the basic features of transition in classical shear flows, including their convective growth rates, inherent three-dimensionality, onset at Reynolds numbers in accord with experimental observations and flow features in accord with early transitional flows. These instabilities have been analyzed both by direct numerical simulation of the evolving three-dimensional flow and by a linear perturbation analysis of the nonparallel two-dimensional (nonlinear travelling wave) flow. In fig. 1, we show the streamlines of a typical two-dimensional base state (here for plane Poiseuille flow at $R = 4000$). The nonparallel character of the base flow leads to considerable complication in its linear stability analysis (see [6] for the formulation of these large-matrix eigenvalue problems). A topic of much current research interest is the development of efficient numerical methods for finding eigenvalues of the very large matrices encountered in problems of this sort. In fig. 2, we give a stability diagram for this transitional instability; here we plot contours of constant growth rate as a function of the amplitude of the two-dimensional base state and the Reynolds number. The growth rates of this instability are $1 \div 2$ orders of magnitude larger than those of Orr-Sommerfeld modes. The
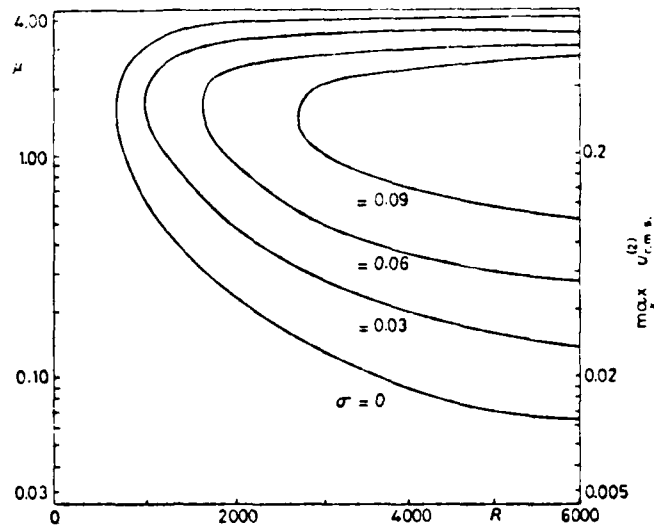
Fig. 2. – Contours of constant growth rate (labelled by growth rate) as a function of R and the amplitude of the background two-dimensional nonlinear wave (see right-hand scale).

development of this three-dimensional secondary instability seems to be consistent with available experimental data on early transitional flows. In fig. 3, we compare contours of the x velocity at the so-called one-spike stage of transition in plane Poiseuille flow obtained a) experimentally by NISHIOKA, IIDA and KANBAYASHI [7] and b) numerically by KLEISER and SCHUMANN [8]. The
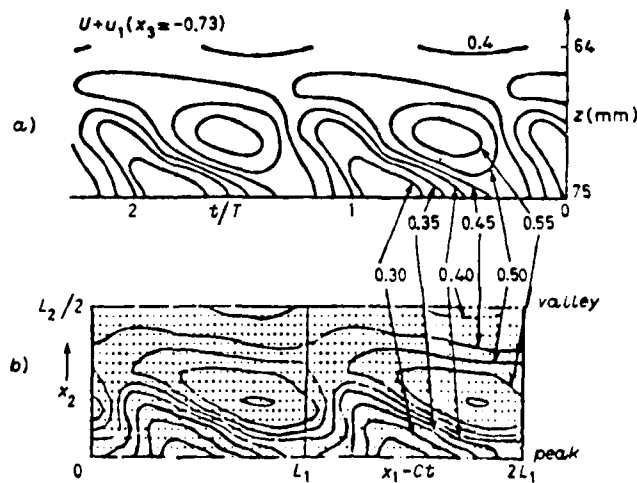
Fig. 3. – Contours of x velocity in the (x, y)-plane at the one-spike stage in the laboratory experiments of Nishioka et al. (a)) and in the numerical simulation of Kleiser and Schumann (b)) (from [8]).

flows that develop from the initial linear instability appear to lead directly to chaos and turbulence and not to saturate into ordered, laminar flow states. Similar instabilities have been found in boundary layers, plane Couette flow, pipe Poiseuille flow (see [6]) and in free shear flows (see [4]).

2'2.4. Competition between two-dimensional pairing and three-dimensional instabilities. Inflectional free shear flows, like mixing layers and jets, are inviscidly unstable to two-dimensional disturbances. Squire's theorem implies that these instabilities are strongest when two-dimensional: when these two-dimensional instabilities evolve in time, they saturate into ordered laminar-flow states characterized by large-scale vortical flow structures. These vortical flows may themselves be unstable to subharmonic (pairing) instabilities, in which two (or more) vortices are paired and generate a new larger-scale vortex motion [9]. In these flows, the three-dimensional instability discussed above is also present [10], but it is not necessarily stronger than the pairing instability. However, the three-dimensional secondary instability is effective at much smaller spanwise spatial scales than is the inviscid primary instability and seems to lead directly to chaotic flows [4].
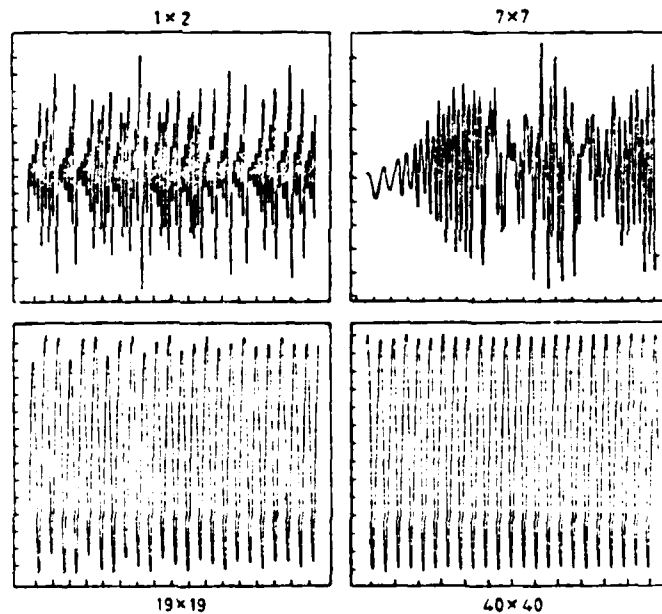

Fig. 4. – Time evolution of the Fourier component b_{02} of the temperature field in two-dimensional Bénard convection at $R_a = 120\,R_{ac}$, $Pr = 20$ [3]. The numbers labelling each plot give the wave number cut-off used to derive the Galerkin approximation to the Boussinesq equations. Thus 1×2 gives the Lorentz equations, while the higher-order models are higher-order Galerkin approximations. Observe that as the resolution increases the chaos disappears.

2'2.5. Spurious (numerical) turbulence. CURRY *et al.* [3] show that, while low-order dynamical systems derived by Galerkin approximation to the two-dimensional Boussinesq equations may exhibit chaotic solutions, this chaos typically disappears as the dimension of the projection space increases (see fig. 4). Similarly, it was shown by ORSZAG and KELLS [5] that under-resolved numerical calculations of transitional planar shear flows may be spuriously chaotic. Under-resolved computations do not have degrees of freedom associated with small spatial scales available to act as an eddy viscosity on well-resolved large scales.

2'3. Computer simulations of turbulence. – In this subsection, I shall give three examples of numerical simulations of turbulent flows. The first two examples, turbulent channel flow and the simulation of a turbulent spot, are of the nature of numerical experiments in which the numericist uses the computer in much the same way as the experimentalist uses the laboratory, namely as a source of data about flows in a controlled environment. The final example, the Taylor-Green vortex, is an example in which the computer is being used to try to uncover fundamental physical laws of turbulence.

2'3.1. Turbulent channel flow. Turbulent channel flows have been simulated numerically three ways: *a*) large-eddy simulation with a subgrid scale turbulence closure for eddies outside the wall layer and a heuristic boundary condition applied at the edge of the viscous sublayer by DEARDORFF [11] and SCHUMANN [12], *b*) large-eddy simulation with a subgrid scale turbulence closure applied to eddies of all scales including those in the wall layer by MOIN and KIM [13] and *c*) full numerical solution of the Navier-Stokes equations by ORSZAG and PATERA [14]. The really crucial differences are, as we again note in subsect. 2'4 below, between *a*) and *b*)-*c*). Simulations of type *a*) have much smaller computational requirements at a given Reynolds number R than either of types *b*) or *c*), the latter requiring asymptotically similar computational work at large R. The deficiency of simulations of type *a*) is that they require modelling of wall layer effects in terms of an over-simplified boundary condition; the deficiencies of types *b*) and *c*) are that, with currently available computer resolution (say $64 \times 64 \times 65$ on a Cray-1 computer), Reynolds numbers are limited to about 10000 (type *b*)) or 5000 (type *c*)). For simulations of types *b*) or *c*), the computational work scales as R^3, so future increases in computer power do little to increase the effective Reynolds number of the computations.

Nevertheless, it is possible to achieve interesting results with full numerical solutions of the Navier-Stokes equations. In fig. 5, we plot the mean velocity profile found in the channel flow computations of Orszag and Patera [14]. The fit to a logarithmic wall layer velocity profile is only marginal, but the resulting von Kármán constant 0.45 is within experimental bounds, so this calculation does give the first computation of a wall layer from the basic prin-
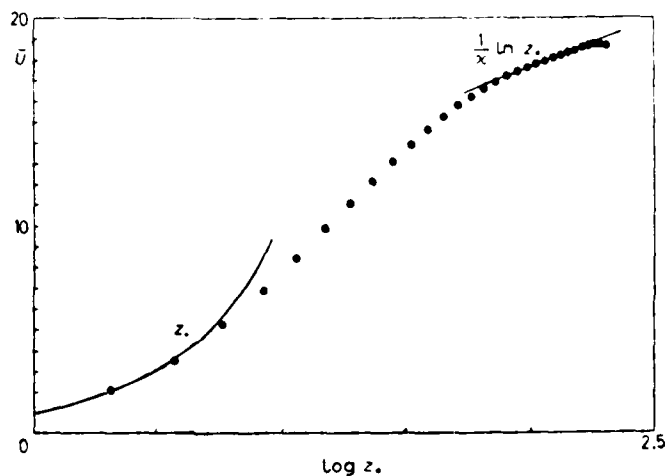
Fig. 5. – Mean turbulent profile obtained by full numerical simulation of plane Poiseuille flow at $R = 5000$ using a $64 \times 64 \times 65$ spectral simulation. Note the viscous sublayer, buffer region and logarithmic layer of $8 \div 9$ data points (from [14]).
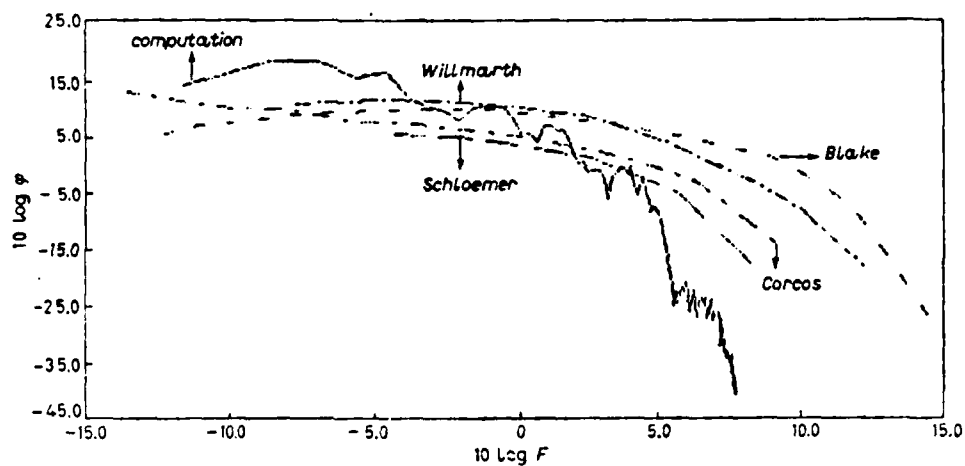

Fig. 6. – A plot of the turbulent wall pressure spectrum as a function of frequency (from [15]).

ciples of fluid dynamics. Another more recent result from computations of this type is given in fig. 6, in which we plot the wall pressure spectrum in a moderate-resolution ($32 \times 32 \times 33$) run compared with available experimental data (see [15]). Despite the moderately low Reynolds number ($R = 5000$) of the simulation, agreement is achieved because flow features that do not depend explicitly on the boundary wall layer structure tend to be Reynolds number independent.

2˙3.2. Turbulent spot. There has been much recent interest in the evolution of localized «spots» in turbulent flows (see [16]). The first numerical simulation of a turbulent spot was reported by LEONARD [17], who used three-dimensional vortex filament techniques to compute the (inviscid) flow. More recently, we have begun a study of spots using full numerical solutions of the Navier-Stokes equations at moderate Reynolds numbers [18]. The latter simulations are performed by forcing the initial flow using a localized force to drive a jet of fluid vertically, then allowing the disturbance to evolve naturally. In fig. 7 and 8, we plot contours of maximum vertical-z velocity in the (x, y) and (x, z) planes at various times of evolution of plane Poiseuille flow. The character of this spot evolution is similar to that observed experimentally: the spot seems to spread in the spanwise direction by «transverse contamination», in agreement with the dye injection experiments of Gad-el-Hak et al. [19]; the greatest turbulent activity is near the edges of the spot, the «spreading» angle of the spot relative to its source is about $10°$, in agreement with the channel flow experiments of Carlson et al. [20]; the vertical structure of the spot is in qualitative agreement with that observed experimentally. Further numerical experiments are under way that should elucidate details of the flow in spots and the surrounding fluid.
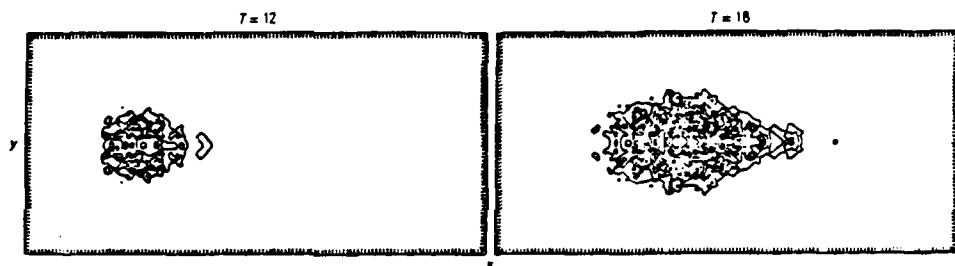

Fig. 7. – Contours of the maximum z-velocity in the (x, y)-plane at $t = 12$, 18 after initializing a turbulent-spot computation by imposed vertical forcing. These computations are performed using a spectral code with 128 $(x) \times 32(y) \times 32(z)$ resolution. Fourier series are used in x and y; Chebyshev polynomial expansions are used in z. Here $R = 6000$.
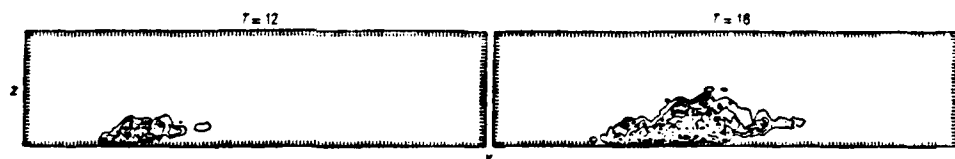

Fig. 8. – Same as fig. 7, except x-z contours of $\max_y |v_z|$.

2˙3.3. Taylor-Green vortex. In order to gain understanding of the basic physics of the generation of small-scale turbulent flow features, a nice

model problem is the Taylor-Green (TG) vortex flow [21, 22]. Here the flow is that which develops in time from initial conditions that consist of excitation in basically a single Fourier mode. Because of nonlinear interaction, the flow becomes strongly three-dimensional and develops excitation at all spatial scales. The TG vortex has been used to study such fundamental questions as the enhancement of vorticity by vortex line stretching, the approach to isotropy of the small scales, possible singular behavior of the Euler equations, formation of an inertial range and analysis of the geometry and intermittency of high-vorticity regions. The TG flow is advantageous for these studies because its special symmetry has allowed the development of numerical algorithms that are a factor 64 more efficient in both memory and storage than conventional periodic-geometry spectral methods. For a three-dimensional flow, this factor 64 translates into a factor 4 increased range of spatial scales—it is now possible to compute the TG vortex flow with $512 \times 512 \times 512$ Fourier modes for each velocity component on the Cray-1 computer (or more than $4 \cdot 10^8$ effective degrees of freedom!).
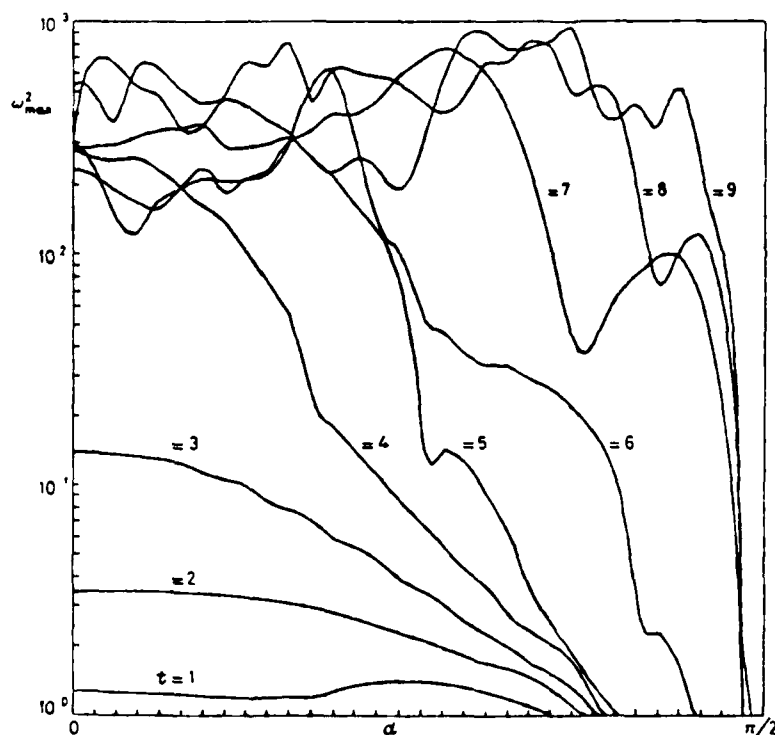

Fig. 9. – A plot of the distribution of large-vorticity regions in the TG vortex flow as a function of time t and distance d away from the side-walls of the impermeable cube in which the flow takes place. Observe how vorticity explodes in towards the center of the cube between $t = 4$ and $t = 8$ (from [22]).

One of the more exciting results to emerge from our studies of the TG flow is the suggestion that viscosity may play an essential role in the development of small-scale turbulence, not just acting as a sink of turbulent kinetic energy. Indeed, we find that the development of the turbulent flow seems to require viscosity to induce instabilities of vortical structures in which the initial large-scale nonturbulent vorticity undergoes an explosive redistribution in space (see fig. 9). These viscosity-induced instabilities are probably effective because viscosity allows vortex line reconnections prohibited in inviscid flow. Similar diffusional instabilities have now been shown to be responsible for the generation of small-scale structures in two-dimensional magnetohydrodynamic [23] and kinetic [24] turbulence. Further study of viscosity-induced instabilities should clarify the development of intermittent flow structures in turbulence.

2'4. *Subgrid scale turbulence closures*. – Perhaps the most distinguishing characteristic of high-Reynolds-number turbulent flows is their large range of excited space and time scales. In homogeneous turbulence, dissipation scale eddies are of order $R^{\frac{3}{4}}$ times smaller than energy-containing eddies. Including the effect of this range of spatial scales on the allowable time step in a numerical solution of the Navier-Stokes equations gives the estimate that order R^3 operations are required to simulate a turbulent flow. This is the reason for interest in the large-eddy simulation method in which excitations on scales smaller than those resolvable numerically are modelled, usually by an eddy viscosity coefficient (see [11, 12]). The basic action of an eddy viscosity on large eddies is reasonable, although it cannot reproduce the random character of the action of small-scale eddies. However, in order to model properly wall turbulence, it is necessary to extend the subgrid modelling ideas of Deardorff and Schumann and treat the turbulence all the way up to a rigid wall, as in recent work by MOIN and KIM [13]. Unfortunately, in order for MOIN and KIM to resolve motions down to the scale of turbulent bursts, which is necessary in order to capture the mechanism producing the turbulence, the work restriction $O(R^3)$ remains. Thus the Reynolds-number restrictions are similar for large-eddy and full numerical solutions of the Navier-Stokes equations that attempt to integrate all the way through the wall layer region.

In recent work, YAKHOT and ORSZAG [25] have used dynamic renormalization group (RNG) methods to treat wall-bounded turbulence. The idea of the infra-red RNG method is to use perturbation methods based on the direct-interaction approximation [26] to eliminate all small spatial scales up to the resolvable grid scale from the Navier-Stokes equations. This is done perturbatively by eliminating narrow bands of wave vectors from the dynamics (see fig. 10), renormalizing the resulting reduced dynamical equation to have the form of the Navier-Stokes equation with modified viscosity and random forcing terms, and then repeating the process iteratively until all the required small scales are removed. The resulting dynamical equations involve a modified

eddy viscosity and a random force, both induced by renormalization. The eddy viscosity is modified from the Smagorinsky viscosity used by DEARDORFF, SCHUMANN and MOIN and KIM in the wall regions in which there is interference between the eddy and molecular viscosities. This interference effect is the key to obtaining a faithful representation of the wall region. Also, the induced
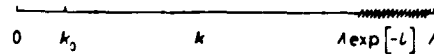

Fig. 10. – A schematic representation of the modal structure of the dynamic renormalization group. Here k_0 represents wave numbers within the energy-containing range, while Λ gives the high-wave-number (viscous) cut-off. Modes in the hatched band are removed at each step of the RNG procedure.

random force is large in the buffer layer between the viscous sublayer and the logarithmic layer, giving a turbulence source in this region. Further work is now under way applying these RNG-based closures to both large-eddy simulations of turbulent shear flows and to the derivation of new classes of turbulence transport (Reynolds averaged) equations that should be useful in engineering applications.

3. – Conclusion.

I have reviewed several areas of activity in the numerical simulation of transition and turbulence in which I have been intimately involved recently. In this short space, it has not been possible to do justice to all of the large number of researchers involved in these fields; the references do a more complete job of surveying the literature. The principal conclusions from our studies are:

   i) Numerical methods now provide essential information complementary to that available from experiment and mathematical analysis.

   ii) Computational fluid mechanics has now matured, so that there are techniques that can be reliably applied to the most difficult of fluid-mechanical problems. In contrast to 10 years ago, it is no longer mainly a question of how to compute a complicated flow, rather, now, it is a question of which flow to compute in order to extract the most useful information.

   iii) It is crucial, especially in our studies of transitional flows, that we have used spectral numerical methods (see sect. 1 above). Spectral methods are so accurate for these problems that we can confidently conclude that properly tested numerical results are true fluid-mechanical results. In contrast to finite-difference or finite-element methods in which an increase in spatial resolution by a factor 2 leads to an error decrease by a factor 4 or 8 or so, with spectral

methods a factor 2 increase in resolution typically decreases the error by several orders of magnitude. This permits accurate verification of results. For example, in recent studies of transition in circular Couette flow, MARCUS *et al.* [27] and MARCUS [28] have been able to achieve at least three-decimal-place agreement with experiment on wave speeds. The confidence in these results has permitted new analytical insights into the character of the onset of wavy instabilities of Taylor vortices in Couette flow [29].

iv) New generations of bigger and faster computers can most profitably be used to extend the range of application of computational fluid dynamics. Transition and turbulence problems in complex geometries with complex physics, like multiphase flows, will surely be the subject of studies in the near future.

* * *

REFERENCES

[1]   D. GOTTLIEB and S. A. ORSZAG: *Numerical Analysis of Spectral Methods: Theory and Applications* (Philadelphia, Penn., 1977).
[2]   D. GOTTLIEB, M. Y. HUSSAINI and S. A. ORSZAG: *Theory and applications of spectral methods*, in *Proceedings of the Symposium on Spectral Methods* (Philadelphia, Penn., 1984), p. 1.
[3]   J. H. CURRY, J. R. HERRING, J. LONCARIC and S. A. ORSZAG: *Order and disorder in two- and three-dimensional Benard convection*, in *J. Fluid Mech.*, to appear.
[4]   M. E. BRACHET and S. A. ORSZAG: *Secondary instability of free-shear flows*, submitted to *J. Fluid Mech.*
[5]   S. A. ORSZAG and L. C. KELLS: *J. Fluid Mech.*, **96**, 159 (1980).
[6]   S. A. ORSZAG and A. T. PATERA: *J. Fluid Mech.*, **128**, 347 (1983).
[7]   M. NISHIOKA, S. IIDA and S. KANBAYASHI: *An experimental investigation of the subcritical instability in plane Poiseuille flow*, in *Proceedings of the X Turbulence Symposium* (Tokyo, 1978), p. 55.
[8]   L. KLEISER and U. SCHUMANN: *Laminar-turbulent transition process in plane Poiseuille flow*, in *Proceedings of the Symposium in Spectral Methods* (Philadelphia, Penn., 1984), p. 141.
[9]   P. C. PATNAIK, F. S. SHERMAN and G. M. CORCOS: *J. Fluid Mech.*, **73**, 215 (1976).
[10] R. T. PIERREHUMBERT and S. E. WIDNALL: *J. Fluid Mech.*, **114**, 59 (1982).
[11] J. W. DEARDORFF: *J. Fluid Mech.*, **41**, 453 (1970).
[12] U. SCHUMANN: *J. Comput. Phys.*, **18**, 376 (1975).
[13] P. MOIN and J. KIM: *J. Fluid Mech.*, **118**, 341 (1982).
[14] S. A. ORSZAG and A. T. PATERA: *Phys. Rev. Lett.*, **47**, 832 (1981).

[15] R. A. HANDLER, R. J. HANSEN, L. SAKELL, E. T. BULLISTER and S. A. ORSZAG: Phys. Fluids, **27**, 579 (1984).

[16] I. J. WYGNANSKI, M. SOKOLOV and D. FRIEDMAN: J. Fluid Mech., **78**, 785 (1976).

[17] A. LEONARD: *Vortex simulation of three-dimensional, spotlike disturbances in a laminar boundary layer*, in *Turbulent Shear Flows*, II, edited by L. J. S. BRADBURY *et al.* (Berlin, 1980), p. 67.

[18] E. T. BULLISTER and S. A. ORSZAG: *Numerical simulation of turbulent spots*, to be published.

[19] M. GAD-EL-HAK, R. F. BLACKWELDER and J. J. RILEY: J. Fluid Mech., **110**, 73 (1981).

[20] D. R. CARLSON, S. E. WIDNALL and M. F. PEETERS: J. Fluid Mech., **121**, 407 (1982).

[21] G. I. TAYLOR and A. E. GREEN: Proc. R. Soc. London, Ser. A, **158**, 499 (1937).

[22] M. E. BRACHET, D. I. MEIRON, S. A. ORSZAG, B. G. NICKEL, R. H. MORF and U. FRISCH: J. Fluid Mech., **130**, 411 (1983).

[23] U. FRISCH, A. POUQUET, P. L. SULEM and U. MENEGUZZI: to be published.

[24] M. E. BRACHET: to be published.

[25] V. YAKHOT and S. A. ORSZAG: *Renormalization group formulation of large eddy simulation*, submitted to J. Fluid Mech.

[26] R. H. KRAICHNAN: J. Fluid Mech., **5**, 497 (1959).

[27] P. S. MARCUS, S. A. ORSZAG and A. T. PATERA: *Simulation of circular Couette flow*, in *Proceedings of the VIII International Conference on Numerical Methods in Fluid Dynamics*, edited by E. KRAUSE (Berlin, 1982), p. 371.

[28] P. S. MARCUS: to be published.

[29] B. J. BAYLY and P. S. MARCUS: *Analytic computation of Taylor-Couette wave speeds*, to be published.

END
DATE
FILMED

5-88

DTIC